공학박사 학위논문

Analysis of desorption behavior in metal-based hydrogen storage systems through pilot-scale experimentation and numerical simulation

실험 및 전산모사를 통한
금속수소화물 수소저장 시스템의 수소 방출 거동 분석

2017년 2월

서울대학교 대학원

재료공학부

오 상 근

Analysis of desorption behavior in metal-based hydrogen storage systems through pilot-scale experimentation and numerical simulation

실험 및 전산모사를 통한 금속수소화물 수소저장 시스템의 수소 방출 거동 분석

지도교수 이 경 우

이 논문을 공학박사 학위논문으로 제출함

2017 년 2 월

서울대학교 대학원

재 료 공 학 부

오 상 근

오상근의 박사학위논문을 인준함

2017 년 2 월

위 원 장	윤 재 륜	(인)
부 위 원 장	이 경 우	(인)
위 원	이 정 중	(인)
위 원	조 성 욱	(인)
위 원	조 영 환	(인)

Abstract

Hydrogen storage alloys that form metal hydrides (MH) are a promising type of material in hydrogen storage applications, allowing for low-pressure, high-density hydrogen storage. However, while many studies are being performed on enhancing the hydrogen storage properties of such alloys, there has been little research on large-scale storage vessels which make use of the alloys. In particular, large-scale, high-density storage devices must make allowances for the temperature variations caused by the heat of reaction between hydrogen and hydriding alloys, which may impact the storage characteristics.

In this study, we propose a numerical model for the design and evaluation of hydrogen storage devices using hydriding alloys. Hydrogen desorption reaction behavior for an alloy is measured in terms of temperature, reaction rate and hydrogen concentration variation over time These data are then analyzed to yield a behavioral correlation which is used as the basis for a comprehensive simulation model of the alloy system. While a solid solution TiCrV-Fe alloy is used in the present study to gather these experimental data, the experimental procedure may be applied in an identical way to any metal hydride material subject to analysis.

Calculated results of the model are found to be in good agreement with experimentally measured data. The accuracy of the model makes it useful in predicting the desorption behavior for a single system under multiple operating conditions. It can also be employed to evaluate multiple systems that satisfy a single

set of given operating conditions.

Given its accuracy and versatility, the model is expected to be highly useful in analyses of multiple system geometries, scales, and metal hydride alloy materials.

Keywords : **hydrogen storage, metal hydride, numerical analysis, numerical modeling, numerical simulation**

Student number : 2006-20859

List of Figures

Chapter 1

Chapter 2

Chapter 3

Chapter 4

Chapter 5

List of Tables

Contents

Chapter 1. Introduction

1.1 The Hydrogen Economy

Hydrogen is a promising energy carrier for the future [1]. Given global concerns over issues such as environmental pollution and the need for a stable and diversified energy supply, an energy economy based on hydrogen produced from renewable energy sources is a key potential solution [2].

The components of a hydrogen economy comprise a hydrogen production system, a hydrogen storage and delivery system, and an energy conversion system to be employed by the end user [1-4]. Among these, the present study is primarily focused on the storage of hydrogen.

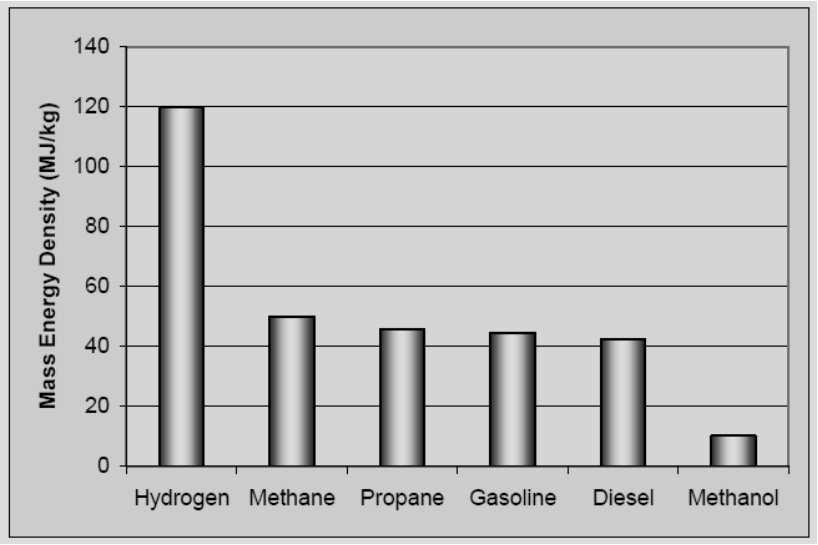

Figure 1-1 Gravimetric energy density of hydrogen

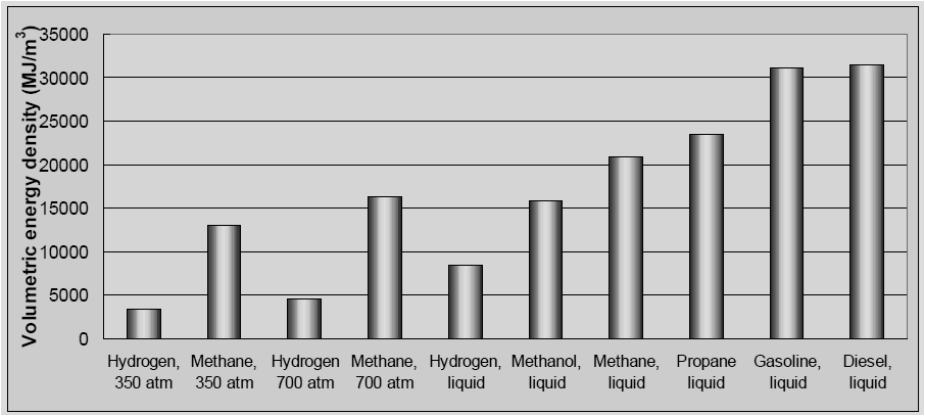

Figure 1-2 Volumetric energy density of hydrogen

1.2 Hydrogen storage methods

An effective strategy for hydrogen storage must take into account its unique physical properties. Hydrogen boasts a high gravimetric energy density compared to conventional modern fossil fuels such as gasoline, diesel or coal, as shown in Figure 1-1. However, whereas most conventional fuels are in a liquid or solid state at ambient temperature and pressure conditions, hydrogen is a lightweight gas. It therefore has a lower energy density per volume than almost any other fuel, as shown in Figure 1-2, and is not as easily handled [1].

Hydrogen can be stored physically as a compressed gas, or as a liquid at very low temperature (20K). These options are relatively well-established, but they are limited in terms of volumetric energy density and stability [2-5].

Alternatively, and perhaps most promisingly, hydrogen can also be stored in a solid state, through the use of materials such as metal hydrides. Major advantages of such an approach include higher volumetric energy densities and greater stability. While there are obstacles to be addressed in terms of gravimetric energy density and cost, active research is being performed on

solid state hydrogen storage due to its high potential for success [1-5], and it is this method that the present study aims to address.

1.2.1 Physical storage of hydrogen

Storage as compressed gas

Currently, storage of hydrogen as a compressed gas is one of the most widespread storage technologies, largely due to its relative conceptual simplicity [2-6]. It involves storing hydrogen at high pressure in high-strength tanks, with the material and design of the tanks selected on the basis of stability and durability [7]. An example of a commercially available compressed hydrogen gas storage vessel is shown in Figure 1-3 [6].

Even the most advanced compressed gas hydrogen storage systems are of relatively simple design, consisting just two primary components. The first is a liner which acts as barrier against hydrogen permeation. The second is a high-strength load-bearing structure which is aimed at securing the tank's mechanical integrity [2-3].

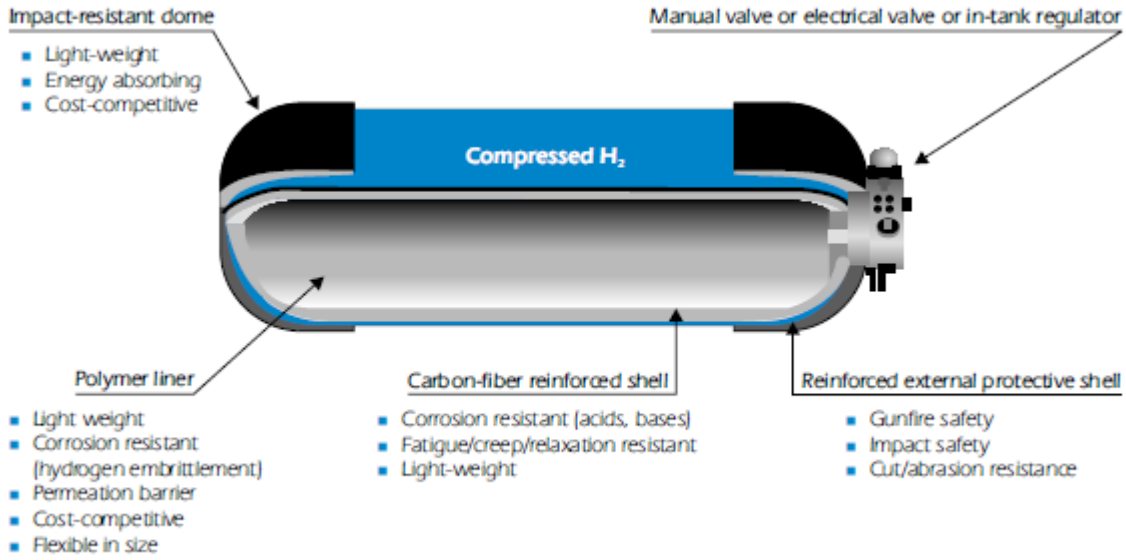

Figure 1-3 Example of commercial compressed hydrogen gas vessel

While the simplicity of these tanks and the consequent ease of their manufacture make them immediately attractive, their use is limited in many applications due to their low volumetric energy density [2-3]. Even at pressures as high as 700 atm, the volumetric energy density of compressed hydrogen gas remains much lower than liquid fuels such as gasoline or propane, and even compared to other gas-state fuels such as methane. This makes them problematic for large-scale commercialization [8].

Storage as liquid

Storage of hydrogen as a liquid offers the advantage of a much higher volumetric energy density than storage as a compressed gas [2-3]. Moreover, the relatively low working pressure compared to high-pressure gaseous systems allows for weight reduction through the use of light-weight materials. Current technology offers gravimetric energy densities on par with conventional fuel tanks [2].

The cryogenic vessels used for storage of liquid hydrogen generally

make use of metallic materials. The structure consists of a vessel within a vessel, or double walls containing an insulation layer between them [2-3, 9]. The design of these vessels require considerations to minimize thermal losses through the effects of thermal radiation, thermal convection and thermal conduction. The inner vessel which actually contains the hydrogen is insulated using a multi-layered material acting as a thermal barrier. This inner vessel is mounted within the outer vessel, and the volume between the two vessels is evacuated to prevent the leakage of heat by thermal convection through 'vacuum super insulation.' An example of a commercially available liquid hydrogen storage vessel is shown in Figure 1-4 [2, 9].

Despite its advantages in terms of energy density, liquid storage of hydrogen has the critical drawback of requiring energy to liquefy the gas. Even after cooling, strict control measures are required to maintain a stable temperature and avoid the risk of overpressure. This can be especially problematic in that for practical use, the fueling equipment and transferring lines must all be heavily insulated as well [1-3].

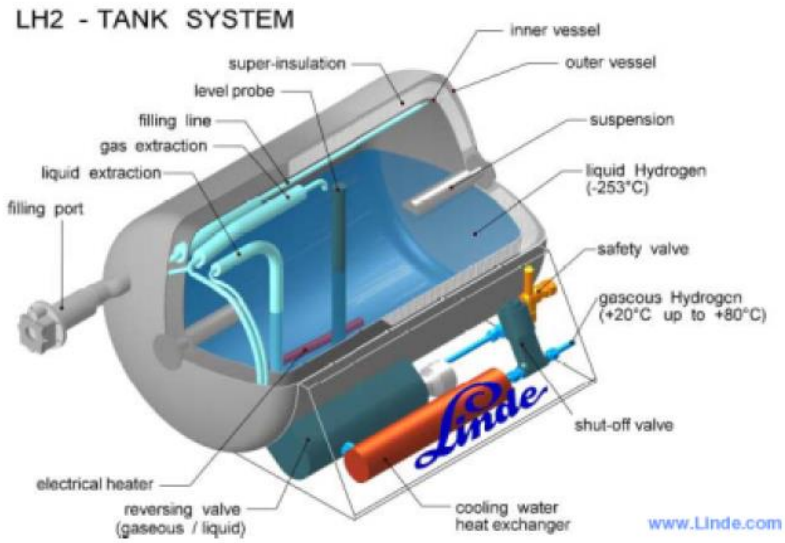

Figure 1-4 Example of commercial liquid hydrogen storage vessel

1.2.2 Metal hydride (MH) materials

Hydrogen storage in metal hydride (MH) materials makes use of metallic alloys which act like sponges that absorb gaseous hydrogen [2, 28]. The storage of hydrogen in hydriding alloys presents an alternative to conventional physical storage, with notable benefits such as a high volumetric density and improved stability. It is worth noting that the release of stored hydrogen is an endothermic process and therefore requires heat, which adds to the storage system's safety [10-12].

The basic underlying principle of the hydriding and dehydriding of metals is relatively simple, and given as:

$$M + \frac{x}{2}H_2 \leftrightarrow MH_x \qquad (1\text{-}1)$$

Storage takes place in the form of solid metal hydrogen compounds formed by an exothermic chemical reaction under hydrogen pressure [12]. The process is illustrated in Figure 1-5. A hydrogen molecule in a gaseous state approaches the metal surface (a). It is attracted to the metal surface by Van der Waals force, leading to a physisorbed state (b). The hydrogen molecule is then dissociated as strongly bound, individual hydrogen atoms by chemisorption (c). Finally,

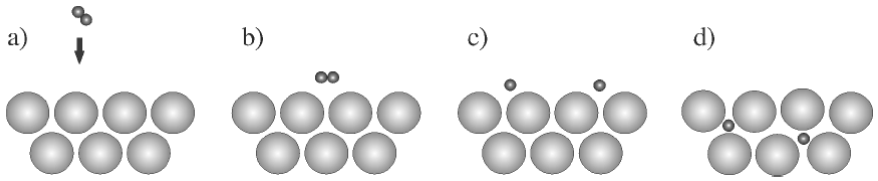

Figure 1-5 Process of hydrogen storage in metal hydride materials

after dissociation on the metal surface, the hydrogen atoms diffuse into the bulk to form a M-H solid solution (d). The stored hydrogen can then be released by applying heat to the material, or by reducing the pressure [12-13].

Materials characterization

The most commonly used representation of a metal hydride material's PCT properties is the isothermal P-C hysteresis loop, a generalized form of which is shown in Figure 1-6 [12].

The material's hydrogen capacity can be defined in a variety of ways. The reversible capacity, or $\Delta(H/M)_{rev}$, is the amount of hydrogen which can be repeatedly stored and released, and can be approximated by the plateau width. For many materials, this capacity is significantly lower than the maximum capacity, or $\Delta(H/M)_{max}$, For most cases, engineering capacity is usually somewhere between $\Delta(H/M)_{rev}$ and $\Delta(H/M)_{max}$. Capacity can be listed in terms of either the atomic ratio of H/M or the weight percent. Both H and M are included in the denominator when calculating the weight percent [12].

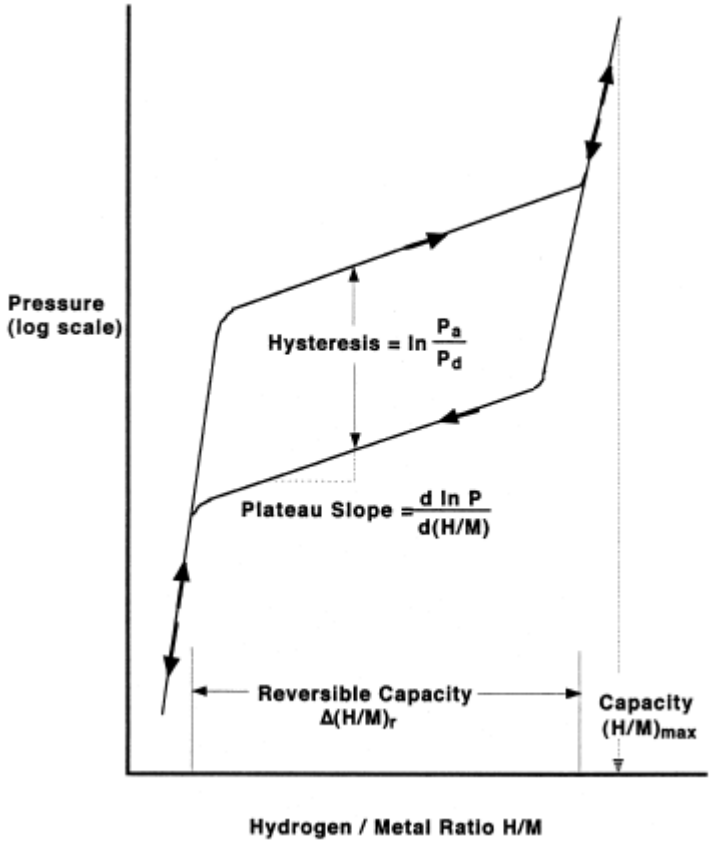

Figure 1-6 Generalized isothermal P-C hysteresis loop

As a plot such as the one in Figure 1-6 is an isothermal P-C loop, the plot must change depending on the temperature. Thermodynamics dictate that as the temperature increases, so too does the plateau pressure. This relationship can be given by the van't Hoff equation:

$$\ln P = \frac{\Delta H}{RT} - \frac{\Delta S}{R} \qquad (1\text{-}2)$$

where ΔH and ΔS are respectively the enthalpy and entropy changes of the reaction, T is temperature and R is the gas constant [12].

For most hydrides, both ΔH and ΔS are negative values, which means that hydrogen absorption is an exothermic process, and hydrogen desorption is an endothermic one. The van't Hoff plot, shown in Figure 1-7, is a graphical representation of pressure versus temperature, and hence acts as a convenient way to analyze a material's thermal stability [12-13].

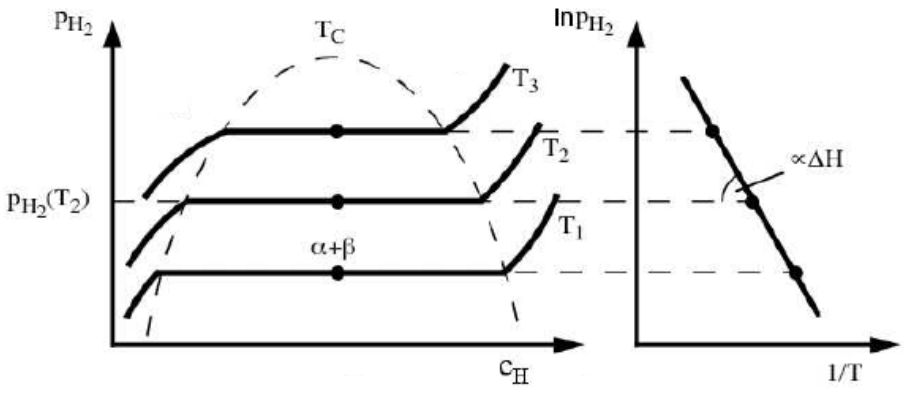

Figure 1-7 Generalized van't Hoff Plot

1.3 Previous Studies

Earlier investigations into the use of metal hydride-forming alloys for the storage of hydrogen can be largely divided into two categories: development of suitable alloys with desirable hydrogen storage properties, and attempts to employ such materials within vessels and storage systems. The following section is a brief overview of such studies, aimed at providing context for the motivation of the present study.

1.3.1 Hydrogen storage alloy development

Several factors must be considered in the selection of the metal alloys for hydrogen storage. They must provide a high gravimetric hydrogen capacity, and be operable at close to ambient temperature conditions. In terms of kinetics, the hydrogen absorption rate and especially the rate of hydrogen release must be rapid enough for engineering purposes. Additionally, the process of hydrogen absorption and release must be repeatable, with no significant loss of storage capacity after multiple cycles [2-3, 5].

A vast number of candidate materials has been investigated as potential hydrogen storage materials. For example, Figure 1-8 shows hydrogen gravimetric capacity as a function of hydrogen release temperature for many of the unique hydrogen storage materials investigated by the Fuel Cell Technologies office of the U.S. Department of Energy [14-15].

Reversible hydrogen storage in metal alloys generally involves the combination of strong hydride-forming elements (A) with weak hydride-forming elements (B) to form the alloys, especially intermetallic compounds. These intermetallic compounds can be categorized as AB_5 intermetallic compounds, AB_2 intermetallic compounds, AB intermetallic compounds and A_2B intermetallic compounds. Several solid solution alloys have also been found to form reversible hydrides, especially alloys based on the solvents Pd, Ti, Zr, Nb and V [12].

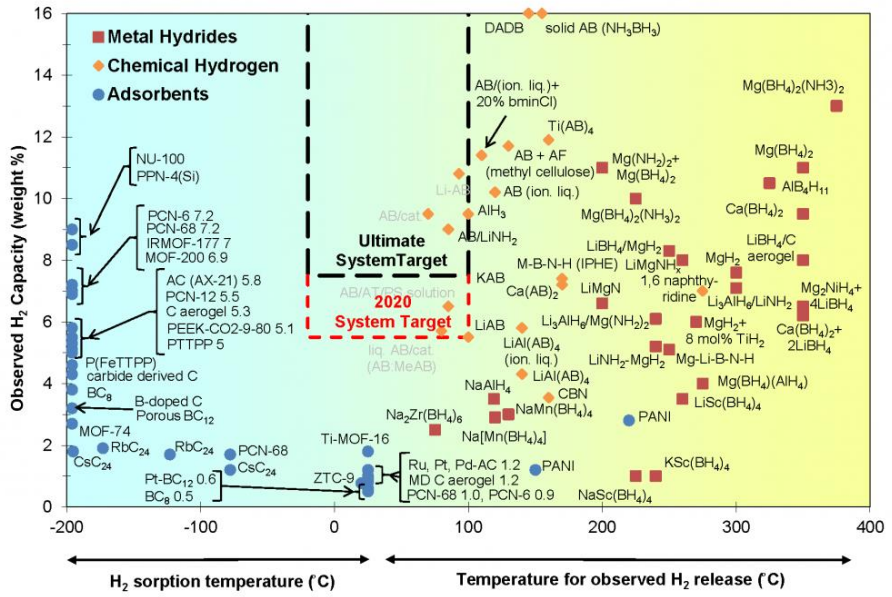

Figure 1-8 Hydrogen storage materials investigated by the U.S. D.O.E.

Intermetallic compounds

The PCT properties of the AB_5 hydriding intermetallics at near-ambient conditions were discovered accidentally at Philips Eindhoven in 1969 while studying the magnet alloy $SmCo_5$. Many different elemental species can be substituted into the A and B lattice sites, lending the family of alloys high versatility [12, 16].

AB_5 alloys demonstrate a broad range of PCT versatility and staability. However, hydrogen capacity tends to be rather low, generally not exceeding a reversible capacity of 1.3 wt %. Moreover, the cost of raw materials is somewhat high [12, 16-19].

Like the AB_5 alloys, AB_2 intermetallic alloys comprise a versatile group of hydride-forming materials whose PCT properties demonstrate potential for hydrogen storage at or near ambient temperature. The Internet database presently contains approximately 500 AB_2 entries, including data from multiple studies [20]. The maximum hydrogen capacities of AB_2 alloys are higher than those of AB_5 alloys, but the reversible capacities are roughly

comparable. They demonstrate a cost advantage, especially if the A-element is mostly Ti [12, 20-30, 35].

TiFe-based AB alloys have good PCT properties salient to engineering purposes, high hydrogen capacities and low raw materials costs. However, problems associated with their activation, gaseous impurities and upper plateau instabilities make them unsuitable for commercial use [31-33, 35].

A_2B compounds, while extensively studied since the 1960s, are not appropriate for use in the desirable range of 0 to 100^oC temperature and 1 to 10 atm due to their inherent stability [12, 20, 34-35].

Solid solution alloys

Metallurgically, a 'solid solution alloy' is a material formed by dissolving one or more minor elements (solutes) in a primary element (solvent). They are differentiated from intermetallic compounds in that the solute need not be present at an integer or near-integer stoichiometric relationship to the solvent. Instead, it is present in the form of a random (disordered) substitutional

or interstitial distribution within the basic crystal structure. Several reports have demonstrated that solid solution alloys based on the solvents such as Pd, Ti, Zr, Nb and V form reversible hydrides [12, 20].

One example of such hydride-forming solid solution alloys is the category of Ti–Cr-based solid solution alloys with a BCC structure [36-39]. The effective volumetric hydrogen storage density is about 1.5–2 times higher than that of liquefied hydrogen, but they are limited by relatively low gravimetric storage density and significantly tilted desorption plateau regions of their *P–C* isotherms, as well as relatively slow reaction rates. Multiple studies have attempted to address these problems [40-47]. Cho et al. reported on the effects of heat treatment on the *P–C* isotherm plateau [40]. Tominaga et al. suggested optimum conditions for the heat treatment [41]. Also in the literature are reports on the effects of additional alloying elements [42-44] and melt-quenching rates [45].

1.3.2 MH-based hydrogen storage systems

Despite the active studies being performed on materials for metal hydride hydrogen storage, only a comparatively limited amount of research has been done on the bulk behavior or storage device designs for such materials in large-scale applications.

Moreover, due to constraints arising from factors such as high cost and practicality, production of large amounts of alloys and direct experimentation on multiple devices which make use of such alloys are prohibitively difficult unless a justifiably effective design is pre-determined. Thus, insightful studies regarding the impact of various functioning variables such as methods for heat management on device efficiency may still be limited to a single design [48-55].

A convenient and reliable alternative to such direct experimentation is to predict the characteristics of various designs through numerical simulation. A number of such studies have been reported in the literature [49-53]. A limitation found in the majority of such studies, however, is that many reported

results derived from numerical analysis are aimed more at evaluating a proposed system, instead of offering a new design direction.

Additionally, the majority of previous reports on the analysis of MH hydrogen storage systems through numerical simulation are based on direct simulations of the interaction between MH materials and hydrogen. This is made problematic by the following two issues.

Porous Media

The conventional models for analyzing hydrogen storage devices that make use of hydriding alloys involve a consideration of both the solid and gas phases that make up the bulk of a porous material, complicating the modeling process. In real-world applications, hydrogen storage alloys are generally used in the form of a powder, which increases the surface area and decreases the distance by which hydrogen atoms must diffuse through the lattice [2, 4, 12-13]. However, numerical analysis of porous media is complicated by the fact that the properties of porous media vary significantly depending on a complex

set of variables. These include the respective properties of the solid and gas phases, the particle size and shape, the porosity (that is, the volume ratio of the gas phase), and the degree of packing [55-58].

In particular, the effective thermal conductivity of a porous bed is of great importance in analyzing hydrogen storage devices that contain alloys in powder form [59]. The generation, absorption and transport of heat all have a significant impact on the material's behavior [59-66], and in this the thermal conductivity plays a critical role.

Numerous methods have been presented to determine effective conductivity of porous media [55, 59, 67-73]. Klein et al. [55] presented a model to calculate the effective thermal conductivity by assuming two half-spherical particles in contact, and using a deformation factor to account for the change in shape under stress. The effective thermal conductivities of metal-hydride beds has also been calculated through a method of homogenization, taking into account variables such as pulverization, void fraction, and contact

area [72-73]. However, given the complexity of variables that influence the effective value, it is difficult to say that any one method is the most suitable.

Reaction Kinetics

In addition to the complications of porous media in a numerical model, conventional models for analyzing hydrogen storage devices that make use of hydriding alloys must also account for the reaction kinetics [59].

The chemical kinetics of the hydriding and dehydriding processes are in most cases described by an Arrhenius equation [74]. This is somewhat limited by the need for a reaction constant, which is dependent on temperature and pressure conditions and difficult to obtain through experiments. Asakum et al. used what is known as the shrinking core model, in which a chemical reaction progresses from outside a spherical reactant to the inside, to analyze the hydriding and dehydriding of the hydrogen storage material [72]. The pressure inside the hydride bed is required in these models, and is obtained indirectly from the temperature through the van't Hoff equation (1-2). Gadre et

al. [64] used of a simple numerical model to obtain relatively good agreement with experimentally measured results in the prediction of discharge behavior from a metal hydride bed. Askri et al. [74] examined whether it is possible to ignore radiation heat transfer, in particular for LaNi5 and magnesium hydride systems, and also reported on hydrogen flow and heat transfer in a metal-hydride bed. Guo et al. [75] investigated the importance of conjugate heat transfer between gas-phase convection and solid-phase conduction.

While these studies have produced meaningful and accurate results, their methods of calculation require potentially inaccurate numerical reflections of porous media, and constants obtained through experiments, the delicacy of which could lead to inaccurate values and skewed results.

If a convenient way to characterize the hydrogen desorption behavior of an MH alloy on a bulk scale were to be established, while addressing the issues that emerge in conventional numerical models, it would allow for a versatile simulation model applicable to various MH materials and hydrogen storage systems which employ such materials.

1.4 Research goals

The goal of the present study is to develop a numerical model of hydrogen desorption behavior in metal hydride hydrogen storage devices. The model is intended for reliable analytical use, while addressing the limitations of earlier numerical studies. As such it is to be applicable not only to analyzing and evaluating a proposed or pre-existing system, but to designing new ones and predicting their performance.

The model is to be based on experimentally measured properties of the material in question. The numerical characterization of the material based on the measured data is to be considered on a bulk scale. The volume occupied by the powdered hydrogen storage alloy will be considered not as a region of porous media comprising both solid and gas phases, but as a single homogenous region with uniform properties throughout. This approach will enable the numerical model to avoid the complications and inaccuracies arising from consideration of porous media, and to eliminate the experimental difficulties associated with models which address desorption reaction kinetics between the

two phases directly.

Despite this simplification, the model must take into consideration the major relevant variables related to the desorption behavior, including the heat of metal-hydrogen reaction and the Pressure-Composition-Temperature properties of the material in question, as well as the material's basic physical properties.

To verify the model's accuracy, numerical simulation results must be compared with data measured from a pilot system. Through such verification of its predictive and analytical capabilities, the model may be expected to be applied to multiple system geometries, scales, alloy compositions and applications.

Chapter 2. Numerical Model Development

2.1 Calculation algorithm

The reaction heat of hydrogen absorption or desorption to or from an MH material will result in a change of material's temperature. This will in turn influence the reaction rate, which is dependent on temperature [5, 12]. The transfer of heat takes place through two major mechanisms: it is transferred within the bulk of the device by thermal conduction, and either introduced to the system or released to the surrounding atmosphere by convective heat transfer at the system boundary.

The magnitude of the reaction heat and its correlation with the system temperature and resulting reaction rate are at the core of the model presented in this study. Initial values for concentration, temperature and reaction rate are given for the system. For each time step, the concentration value will decrease depending on the reaction rate. The amount of reacted hydrogen will also determine the reaction heat, which in turn determines the change in temperature.

The new temperature and hydrogen concentration then become the basis for the new reaction rate in the next time step.

Hence, the reaction rate may be defined as a function of temperature and concentration, or

$$R = f(T,C) \qquad (2\text{-}1)$$

where R is the reaction rate, T is the temperature, and C is the hydrogen concentration.

While this relationship may be determined experimentally for any MH alloy, in some cases the variable C has only a negligible effect on the reaction rate. In such cases, in the interest of calculation efficiency and simplicity, we may omit C from the relationship and define the reaction rate as

$$R = f(T) \qquad (2\text{-}2)$$

This correlation between temperature, concentration and reaction rate is taken from measurements on an experimental system, which will be outlined in the subsequent chapter.

2.1.1 Rate factor ‘k’

The relationship between reaction rate, hydrogen concentration and temperature, in the basic form outlined above, requires that no limitation is placed on the reaction of hydrogen and MH alloy, i.e. any reaction which is allowed by the temperature and hydrogen concentration condition will indeed take place. But in practice, it is far more likely that a user-designated reaction rate will be imposed on the system depending on the amount of hydrogen gas which is required for the application over time [2-3, 10].

To account for this, we implement a variable 'k' which is to be called the 'rate factor.' Additionally, to account for local variations, we distinguish between R, the reaction rate for any given cell in a model system, and Q, the total flow rate which results from the system as a whole.

The potential total flow rate which temperature and concentration conditions allow is called Q_P, and is defined as

$$Q_P = \frac{\sum f(T_i, C_i) \times V_i}{\sum V_i} \qquad (2\text{-}3)$$

where T_i, C_i and V_i respectively represent the temperature, hydrogen concentration and volume of each cell with index i.

The real total flow rate which actually occurs, the maximum value for which is a user designated value Q_{max}, is then given as Q_R, and defined as

$$Q_R = k \times Q_p \qquad (2\text{-}4)$$

thus giving us the definition for the rate factor, k, as

$$k = Q_R / Q_P \qquad (2\text{-}5)$$

Hence, if $k < 1$, the reaction occurs at a rate lower than the temperature and concentration allow. The real flow rate under this condition is the user-designated maximum value Q_{max}.

As the desorption reaction continues, Q_P will decrease over time and the value of k will approach 1. When $k = 1$, the flow rate allowed by the temperature and concentration is less than the user-designated limit, so that the entire potential flow rate does indeed occur. In such conditions, $Q_R = Q_P$. Since the real flow rate cannot exceed the potential rate allowed by the temperature and concentration, it stands to reason that k cannot ever exceed 1.

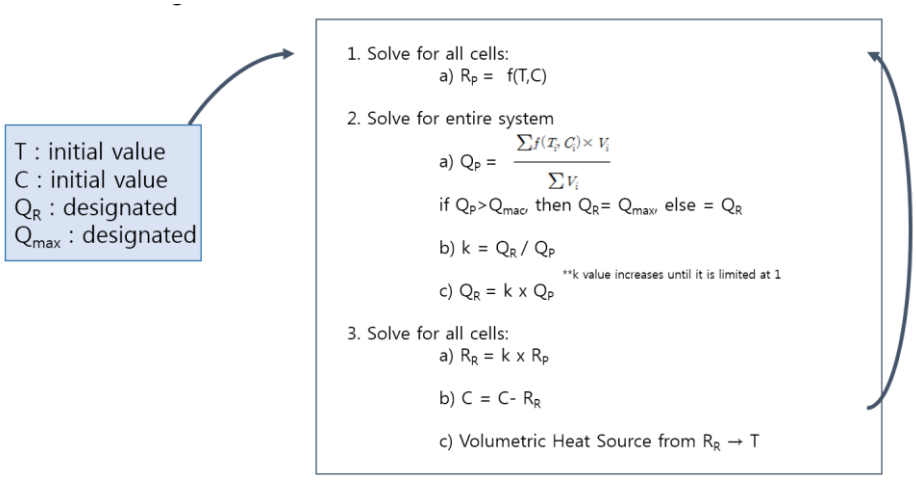

Figure 2-1 Schematic outline of model algorithm

2.1.2 Order of calculation

The model is calculated according to a comprehensive algorithm as represented schematically in Figure 2-1. The calculation is carried out in the following order:

1. Initial values are given for the temperature T, hydrogen concentration C, potential reaction rate R_P (as defined by R=f(T,C)) and real total flow rate Q_R (initially = Q_{max})

2. For the entire system,

a. $Q_p = \dfrac{\sum f(T_i, C_i) \times V_i}{\sum V_i}$

from equation 2-1, $R_P = f(T_i , C_i)$ for a cell with index i

b. $k = Q_r / Q_p$

if $k < 1$, $k_{n+1} = k_n$ (where n is the time step number)

if $k \geq 1$, $k_{n+1} = 1$

c. $Q_R = k \times Q_P$

3. For each computational cell,

a. $R_R = k \times R_P$

b. C diminishes according to R_R

c. Reaction heat is determined by R_R => calculate T

d. $R_P = f(T,C)$ from new T and C values

4. Steps 2-3 are repeated for each time step of the simulation

This algorithm allows us to calculate the transient potential reaction rate, the real reaction rate, temperature and hydrogen concentration for any locality in a system over a period of time.

2.2 Material properties

The major volumetric parameters for the materials considered in this study are density, heat capacity and thermal conductivity. As pointed out in earlier studies [13], metal hydride materials will generally reach a uniform particle size following several cycles of hydrogenation and dehydrogenation, and therefore the powder bed is assumed to be a homogeneous volume of uniform conductivity, density and porosity

Physical properties of porous media

Thermal conductivity κ is a measure of the rate at which heat is transferred through a material. The conductivity is defined by the heat *Q* (not to be confused with the flow rate Q in section 2.1.1) transferred across a given plane of area *A* per unit time in the presence of a temperature gradient [70]

$$\frac{Q}{A} = \kappa \frac{\Delta T}{\Delta X} \qquad (2\text{-}6)$$

The thermal conductivity κ plays a similar role in heat transfer that the diffusion coefficient *D* does in mass transfer.

The effective thermal conductivity of the material, i.e. the rate at which heat can be conducted through the material in its powdered state, is of particular importance in determining the efficiency of a device [48, 59], especially given the unpredictable conductivity of porous materials [59-66].

Even when the thermal conductivity values are known for the two phases that comprise a powder medium, i.e. the solid particles and the gas in the gaps between them, the effective thermal conductivity κ_{eff} of the powder will vary greatly depending on the porosity, the pressure of compaction, if any, and the particle size and shape [58].

Theoretical methods to calculate the effective thermal conductivity do exist. However, due to their relative complexity and unreliability, the effective thermal conductivity value of alloy powder in the present study is taken from measurement of a sample of the material used for the model development. The specific heat is likewise measured experimentally, as well as the heat of reaction per mol H_2. These data, applied as volume conditions in the model, are shown in Figure 2-2.

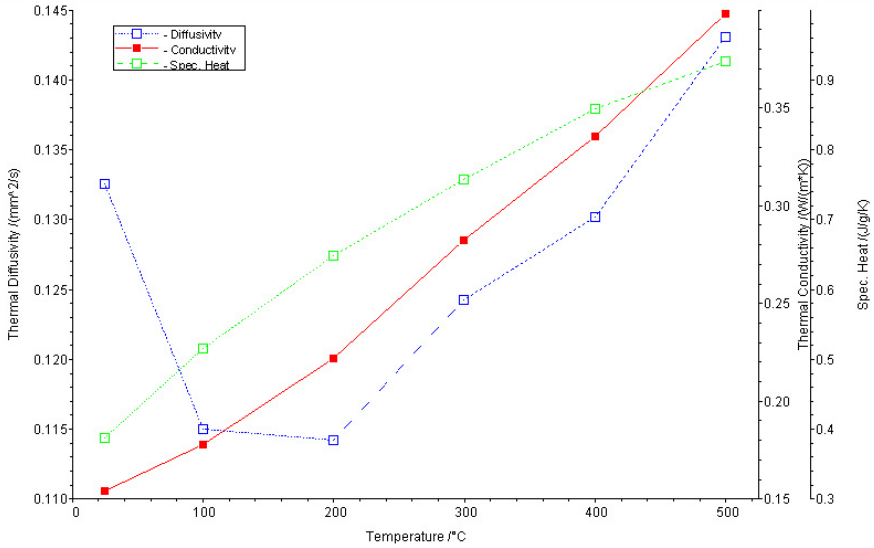

Figure 2-2 Measured physical properties of MH alloy powder

2.3 Numerical calculation theory

In the present study, we use CFD-ACE, a commercial software package for numerical analysis. We employ our own independently developed subroutine in order to reflect the changes in concentration, reaction heat and reaction rate as described in the model above.

2. 3. 1 Flow

The unique algorithm of the model in the present study eliminates the need to account for pressure or the gas phase component of the porous media comprising the hydrogen storage material and the gas in the gaps between the particles. However, the model as a whole must at times account for flow in cases such as the use of fluid-based heat exchange systems or specific storage system designs.

Mass conservation

Conservation of mass requires that the time rate of change of mass in

a control volume be balanced by the net mass flow into the same control volume (outflow - inflow). This can be expressed as:

$$\frac{\partial \rho}{\partial t} + \nabla \bullet (\rho \vec{V}) = 0 \qquad (2\text{-}7)$$

The first term on the left hand side is the time rate of change of the density (mass per unit volume). The second term describes the net mass flow across the control volume's boundaries and is called the convective term [76].

Momentum conservation

Newton's second law states that the time rate of change of the momentum of a fluid element is equal to the sum of the forces on the element.

The x-component of the momentum equation is found by setting the rate of change of x-momentum of the fluid particle equal to the total force in the x-direction on the element due to surface stresses plus the rate of increase of x-momentum due to sources:

$$\frac{\partial(\rho u)}{\partial t} + \nabla \bullet (\rho \vec{V} u) = \frac{\partial(-p + \tau_{xx})}{\partial x} + \frac{\partial \tau_{yx}}{\partial y} + \frac{\partial \tau_{zx}}{\partial z} + S_{Mx} \qquad (2\text{-}8)$$

Similar equations can be written for the y- and z-components of the momentum

equation:

$$\frac{\partial(\rho v)}{\partial t} + \nabla \bullet (\rho \vec{V} v) = \frac{\partial \tau_{xy}}{\partial x} + \frac{\partial(-p + \tau_{yy})}{\partial y} + \frac{\partial \tau_{zy}}{\partial z} + S_{My} \qquad (2\text{-}9)$$

$$\frac{\partial(\rho w)}{\partial t} + \nabla \bullet (\rho \vec{V} w) = \frac{\partial \tau_{xz}}{\partial x} + \frac{\partial \tau_{yz}}{\partial y} + \frac{\partial(-p + \tau_{zz})}{\partial z} + S_{Mz} \qquad (2\text{-}10)$$

In these equations, p is the static pressure and t_{ij} is the viscous stress tensor [76].

Navier-Stokes equations

The momentum equations, given above, contain as unknowns the viscous stress components t_{ij}, therefore a model must be provided to define the viscous stresses.

In Newtonian flows, the viscous stresses are proportional to the deformation rates of the fluid element. The nine viscous stress components (of which six are independent for isotropic fluids) can be related to velocity gradients to produce the following shear stress terms:

$$\tau_{xx} = 2\mu \frac{\partial u}{\partial x} - \frac{2}{3} u(\nabla \bullet \vec{V}) \qquad (2\text{-}11)$$

$$\tau_{yy} = 2\mu \frac{\partial v}{\partial y} - \frac{2}{3} u(\nabla \bullet \vec{V}) \tag{2-12}$$

$$\tau_{zz} = 2\mu \frac{\partial w}{\partial z} - \frac{2}{3} u(\nabla \bullet \vec{V}) \tag{2-13}$$

$$\tau_{xy} = \tau_{yx} = \mu\left(\frac{\partial u}{\partial y} + \frac{\partial v}{\partial x}\right) \tag{2-14}$$

$$\tau_{xz} = \tau_{zx} = \mu\left(\frac{\partial u}{\partial z} + \frac{\partial w}{\partial x}\right) \tag{2-15}$$

$$\tau_{yz} = \tau_{zy} = \mu\left(\frac{\partial v}{\partial z} + \frac{\partial w}{\partial y}\right) \tag{2-16}$$

Substitution of the above shear stress terms into the momentum equations yields the Navier-Stokes equations:

$$\begin{aligned} &\frac{\partial(\rho u)}{\partial t} + \nabla \bullet (\rho \vec{V} u) = -\frac{\partial p}{\partial x} + \frac{\partial}{\partial x}\left[2\mu \frac{\partial u}{\partial x} - \frac{2}{3}\mu(\nabla \bullet \vec{V})\right] \\ &+ \frac{\partial}{\partial y}\left[\mu\left(\frac{\partial u}{\partial y} + \frac{\partial v}{\partial x}\right)\right] + \frac{\partial}{\partial z}\left[\mu\left(\frac{\partial u}{\partial z} + \frac{\partial w}{\partial x}\right)\right] + S_{Mx} \end{aligned} \tag{2-17}$$

$$\frac{\partial(\rho v)}{\partial t}+\nabla\bullet(\rho\vec{V}v)=-\frac{\partial p}{\partial y}+\frac{\partial}{\partial x}\left[\mu\left(\frac{\partial u}{\partial y}+\frac{\partial v}{\partial x}\right)\right]$$
$$+\frac{\partial}{\partial y}\left[2\mu\frac{\partial v}{\partial x}-\frac{2}{3}\mu(\nabla\bullet\vec{V})\right]+\frac{\partial}{\partial z}\left[\mu\left(\frac{\partial v}{\partial z}+\frac{\partial w}{\partial y}\right)\right]+S_{My} \quad (2\text{-}18)$$

$$\frac{\partial(\rho v)}{\partial t}+\nabla\bullet(\rho\vec{V}w)=-\frac{\partial p}{\partial z}+\frac{\partial}{\partial x}\left[\mu\left(\frac{\partial u}{\partial y}+\frac{\partial v}{\partial x}\right)\right]$$
$$+\frac{\partial}{\partial y}\left[\mu\left(\frac{\partial v}{\partial z}+\frac{\partial w}{\partial x}\right)\right]+\frac{\partial}{\partial z}\left[2\mu\frac{\partial w}{\partial y}-\frac{2}{3}\mu(\nabla\bullet\vec{V})\right]+S_{Mz} \quad (2\text{-}19)$$

By rearranging these equations and moving the smaller contributions of the viscous stress terms to the momentum source term, we can rewrite the Navier-Stokes equations in a more useful form:

$$\frac{\partial(\rho u)}{\partial t}+\nabla\bullet(\rho\vec{V}u)=-\frac{\partial p}{\partial x}+\nabla\bullet(\mu\nabla u)+S_{Mx} \quad (2\text{-}20)$$

$$\frac{\partial(\rho v)}{\partial t}+\nabla\bullet(\rho\vec{V}v)=-\frac{\partial p}{\partial y}+\nabla\bullet(\mu\nabla v)+S_{My} \quad (2\text{-}21)$$

$$\frac{\partial(\rho w)}{\partial t}+\nabla\bullet(\rho\vec{V}w)=-\frac{\partial p}{\partial z}+\nabla\bullet(\mu\nabla w)+S_{Mz} \quad (2\text{-}22)$$

[76]

2. 3. 2 Heat transfer

Heat transfer processes are computed by solving the equation for the conservation of energy. This equation can take several forms and CFD-ACE+ numerically solves the energy equation in the form known as the total enthalpy equation. This form is fully conservative and is given in equation (2-23).

$$\begin{aligned}\frac{\partial(\rho h_0)}{\partial t} + \nabla \bullet (\rho \vec{V} h_0) = \nabla \bullet (k_{eff} \nabla T) + \frac{\partial p}{\partial t} \\ + \left[\frac{\partial(u\tau_{xx})}{\partial x} + \frac{\partial(u\tau_{yx})}{\partial y} + \frac{\partial(u\tau_{zx})}{\partial z} \right] \\ + \left[\frac{\partial(u\tau_{xy})}{\partial x} + \frac{\partial(u\tau_{yy})}{\partial y} + \frac{\partial(u\tau_{zy})}{\partial z} \right] \\ + \left[\frac{\partial(u\tau_{xz})}{\partial x} + \frac{\partial(u\tau_{yx})}{\partial y} + \frac{\partial(u\tau_{zx})}{\partial z} \right] + S_h\end{aligned} \qquad (2\text{-}23)$$

Where h_0 is the total enthalpy and is defined as

$$h_0 = i + \frac{p}{\rho} + \frac{1}{2}\left(u^2 + v^2 + w^2\right) \qquad (2\text{-}24)$$

Where i is the internal energy and is a function of the state variables r and T, P is the static pressure and t_{ii} is the viscous stress tensor. k_{eff} is the effective thermal conductivity of the material. In laminar flow, this will be the thermal conductivity of the fluid, k [76].

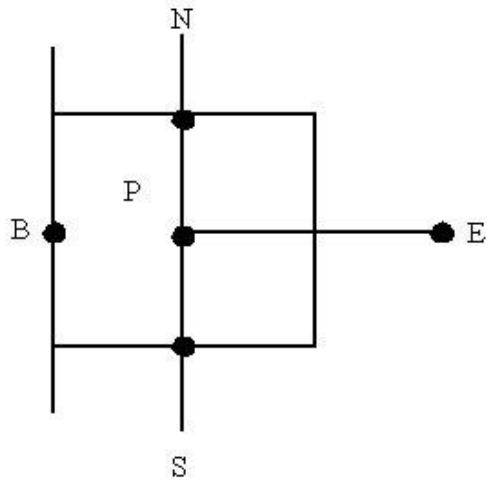

Figure 2-3 Computational boundary cell

2. 3. 3 Boundary conditions

The general treatment of boundary conditions in the finite-volume equations is discussed in this section. A control cell adjacent to the west boundary of the calculation domain is shown in Figure 2-3.

A fictitious boundary node labeled B is shown. The finite-volume equation for node P will be constructed as:

$$a_p\phi_p = a_E\phi_E + a_N\phi_N + a_S\phi_S + S \tag{2-46}$$

Coefficient a_w is set to zero after the links to the boundary node are incorporated into the source term S in its linearized form,

$$S = S_u + S_p\phi_p \tag{2-47}$$

All boundary conditions using this numerical simulation are implemented in this way [77].

Fixed value boundary condition

If the boundary value is fixed as ϕ_B, the source term is modified as:

$$S_U = S_U + a_W\phi_B \tag{2-48}$$

$$S_P = S_P - a_W \tag{2-49}$$

Zero-flux boundary conditions

At zero-flux boundaries, such as adiabatic walls for heat and symmetric boundaries for any scalar variables, the boundary link coefficients are simply set to zero without modifying source terms [76].

Chapter 3. Experimentation

3.1 TiCrV-Fe material

In order to properly develop the model proposed in the present study, direct experimentation using an actual MH alloy needed. This requirement is two-fold. First, there must be a reference material to gather meaningful quantitative data to be applied to the numerical model, especially the relationship between the reaction rate, the hydrogen concentration and the temperature. Secondly, a real experimental system is needed for comparison between measured and calculated behavior. The model's accuracy and reliability must be verified through such a comparison of calculated and measured results for identical operating conditions.

The necessary MH alloy material for experimentation was provided by researchers at the Korean Institute of Geoscience and Mineral Resources (KIGAM). The material was developed based on previous studies on the $Ti_{0.32}Cr_{0.43}V_{0.25}$ solid solution alloy as a potential hydrogen storage material [37, 40, 42, 47, 78-79].

Previous studies found that both the total and reversible hydrogen storage capacities of the alloy as well as the plateau flatness were improved by heat treatment [37]. The effective reversible hydrogen storage capacity remained at approximately 2 wt% after 1000 cycles of pressure swing cyclic tests. The hydrogen storage capacity could also be recovered almost to the initial state by reactivating the alloy [78].

Additional studies found that a fraction of the Cr could be replaced with Mn or a combination of Mn and Fe to increase the hydrogen storage capacity and the plateau pressure of the $Ti_{0.32}Cr_{0.43}V_{0.25}$ alloy. Substitution of Mn alone increased the reversible hydrogen storage capacity, though the plateau pressure showed no significant change. When Fe was added with Mn, however, both the hydrogen storage capacity and the plateau pressure increased [79].

In the present study, the simulations are based on direct experimental measurements of an alloy that was developed as a consequence of the research outlined above. Namely, measurements are taken from the $Ti_{0.32}Cr_{0.35}V_{0.25}$-$Fe_{0.08}$ solid solution alloy, in which a portion of the Cr in the $Ti_{0.32}Cr_{0.43}V_{0.25}$ solid

solution alloy is replaced with Fe. The PCT characteristics of the alloy at various temperatures are given in Figure 3-1. The alloy demonstrates a relatively high reversible storage capacity within a reasonable pressure range. Reaction heat for the alloy considered in this study was measured in samples to be 42 kJ for each mole of reacted hydrogen gas [79].

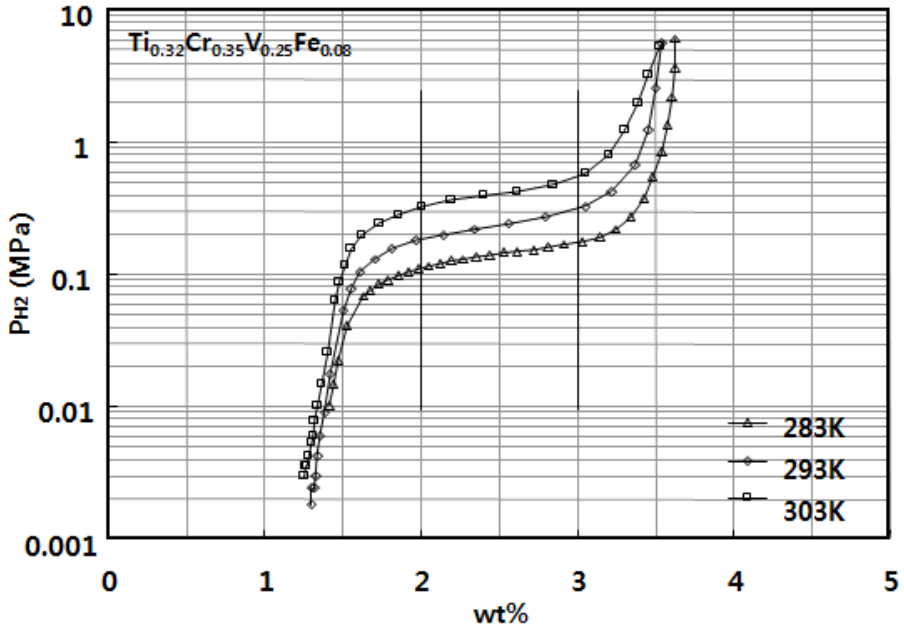

Figure 3-1 PCT characteristics of $Ti_{0.32}Cr_{0.35}V_{0.25}$-$Fe_{0.08}$ alloy

3.2 Materials characterization

The specifics of equations (2-1) and (2-2), that is, the correlation between temperature, concentration and reaction rate, must be taken from measurements on an experimental system using the MH alloy in question.

In order to obtain bulk-scale data of the alloy in question, data must be gathered from an experimentation system with a simple hydrogen storage device. The system, as shown in Figure 3-2, consists of a MH tank filled with approximately 1kg of TiCrV-Fe alloy and a mass flow meter (MFM). The MH tank is composed of stainless steel, and is fitted with metal plates at regular intervals made from stainless steel or copper to aid thermal conduction. Multiple thermocouples placed strategically inside the MH tank make it possible to obtain both localized and average temperature readings from within the tank during operation. Gas desorption flow rates are measured through the mass flow meter.

For an experimental trial, the valve of the MH tank is opened and the hydrogen stored in the alloy is allowed to flow freely. Temperature can be freely

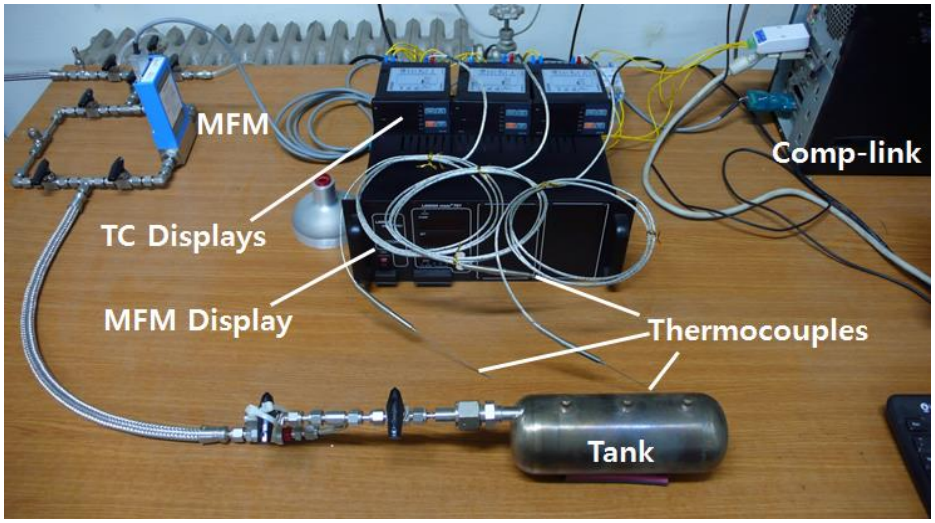

Figure 3-2 Experimental system for material characterization

altered during a trial through the use of devices such as heaters and blowers. The variation of temperature by such additional measures within an experimental trial is of little concern, as the aim of the experimentation is to gather data which will reveal the temperature's relationship not to the time during which the process occurs, but to the concentration and reaction rate, which are also measured over time.

While the reaction rate and temperature are measured in real time, the measurement of concentration requires an additional step. The amount of hydrogen initially stored in the MH tank is a known quantity. Therefore, the concentration over time can be calculated by simply subtracting the reaction amount measured by the MFM for each time step from the concentration value in the previous time step.

To ensure that the data gathered this way and the specifics of equations (2-1) and (2-2) that are drawn from the data are independent of the experimental MH tank, two different tanks of varying design and amount of MH material are used.

3. 3 Experimental verification of model

To ensure that the numerical model is accurate and reasonable, we performed direct experimentation on two pilot tanks under various conditions. As illustrated in Figure 3-3(a), the stainless steel tanks are in the shape of a cylinder. Copper fins are fitted inside, as in Figure 3-3(b) to allow for better heat conduction. The inner interior dimensions of the tanks measure 200 mm high with a radius of 140mm. Each of the tanks is filled with 5 kg of TiCrV-Fe alloy. The tanks can each be used separately, or paired as in Figure 3-4.

The exterior of the tanks is fitted with heaters, which allows for constant regulation of the surface temperature. Reaction rate and resulting gas flow rate are controlled (i.e. limited) through a mass flow controller.

A 3D numerical model grid of the system with 21,920 computational cells was created, a cross section of which is shown in Figure 3-5 with the copper fins and interior of the steel liner shown in dark lines. The algorithm described in Chapter 2 was applied for the various experimentation conditions to compare measured and simulated results.

(a)

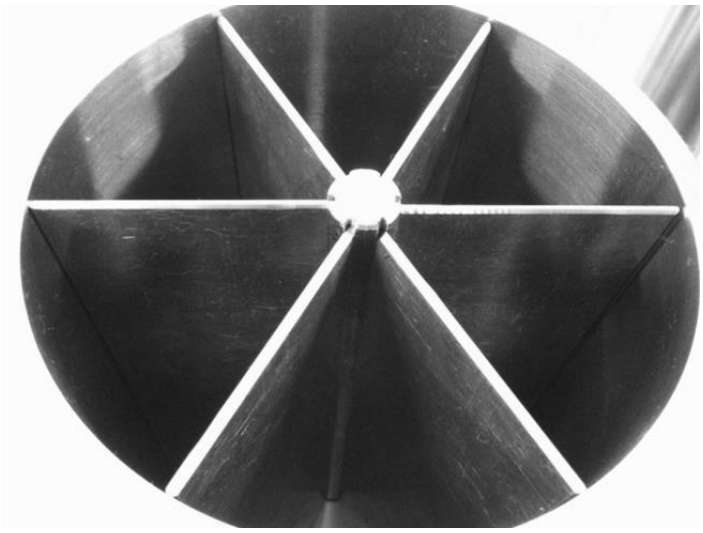

(b)

Figure 3-3 Pilot-scale tanks for model verification

Figure 3-4 Paired, simultaneous use of multiple tanks

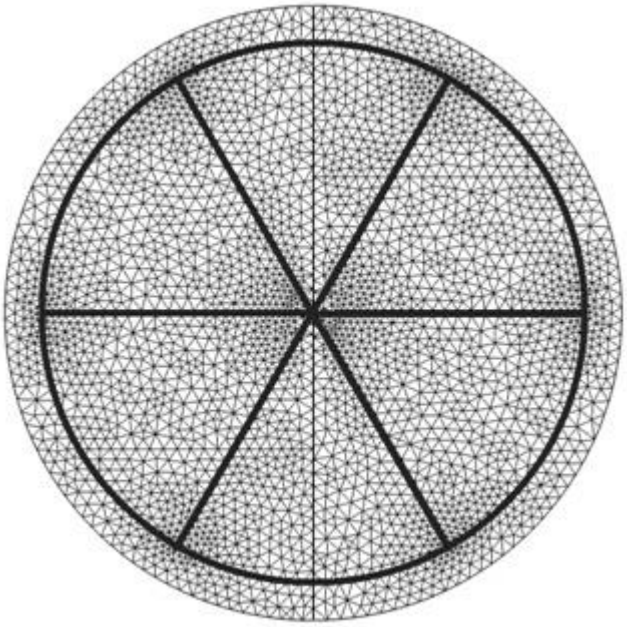

Figure 3-5 Cross-section of 3D numerical model grid of pilot tank

Experiments on the pilot tanks were performed with various set flow limits. The external temperature was kept constant by use of the external heaters. Hydrogen gas desorption and release was allowed up to the limited flow rate starting from an initial charge pressure of 35 atm and pre-heating to make the overall temperature within the tank uniform.

Chapter 4. Results and Discussion

4.1 Numerical characterization of material

The goal of the experiments for material characterization as outlined in Section 3.1 is to obtain a numerical relationship between the reaction rate, hydrogen concentration and temperature which can then be applied to the calculation algorithm for the numerical model, as outlined in Section 2.1

4.1.1 Temperature and reaction rate

Figure 4-1 shows the variation of average temperature within the experimental tank over a period of 5 minutes following the initial release of hydrogen. There is a rapid initial drop in the temperature which can be attributed to two factors.

First, there is a rapid expansion of hydrogen within the tank that exists as a gas, not absorbed within the MH alloy, leading to a drop in temperature. To account for this, which is not related to the desorption behavior of the MH material, data measured within the first several seconds are disregarded.

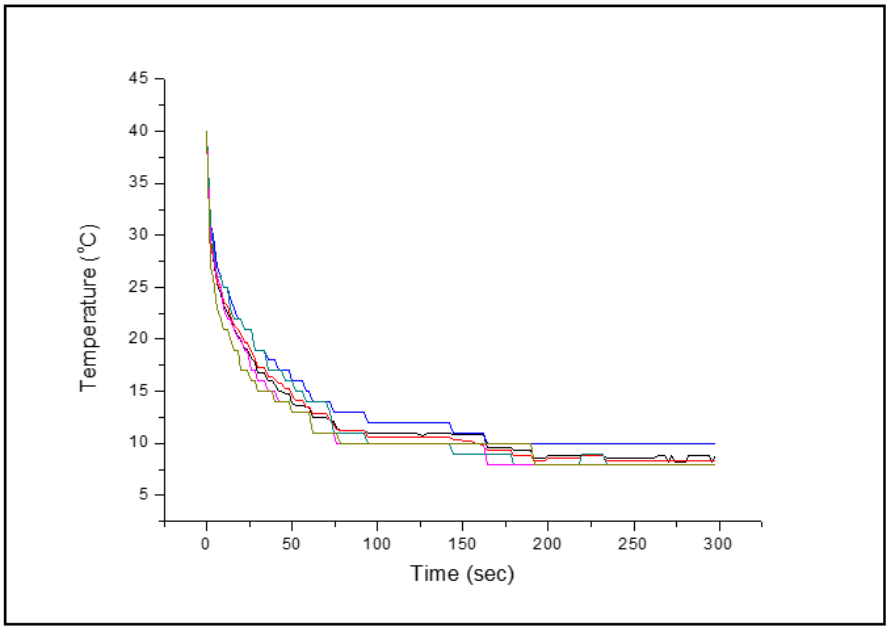

Figure 4-1 Variation of average temperature within experimental tank

Second, the initial value is also the highest for the reaction rate. This means that with the rapid reaction, more reaction head is absorbed in the endothermic process, leading to a more rapid drop in temperature. As the cooler temperatures lead to slower reaction rates, the rate at which the temperature decreases also becomes slower. Eventually, the temperature reaches a steady value, indicating a state in which the heat required for the desorption reaction is in equilibrium with the heat which can be transferred from outside the tank to the MH alloy.

Figure 4-2 shows the measured flow rate per unit mass of the MH material over a period of 5 minutes following the initial release of hydrogen. The flow rate, which in this case is a direct reflection of the reaction rate, is initially high. However, as the system temperature drops, so too does the flow rate. Eventually, the flow rate reaches a steady value, corresponding with the temperature condition in which the heat required for the desorption reaction is in equilibrium with the heat which can be transferred from outside the tank to the MH alloy.

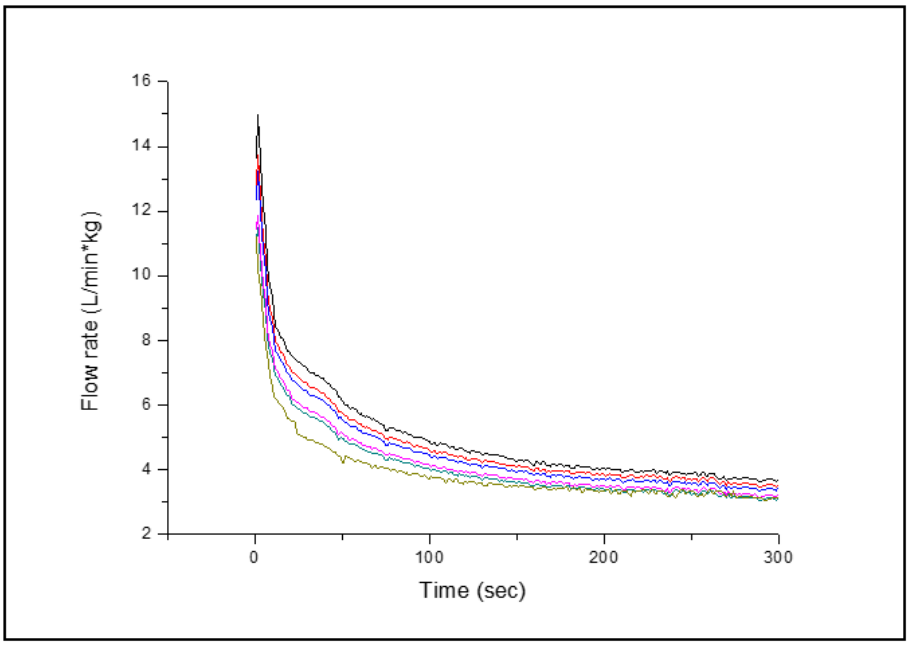

Figure 4-2 Variation of flow rate per unit mass of MH material

4.1.2 The relationship between R, T and C

Multiple sets of the experimental data described in the previous section must next be analyzed to determine what relationship, if any, can be found between the reaction rate, the hydrogen concentration and the temperature.

The measured temperature and reaction rate data exist in relation to the time elapsed during the experimental trial. The hydrogen concentration over time can be calculated by subtracting the reaction amount measured by the MFM for each time step from the concentration value in the previous time step, as explained in Section 3.2

3D data fitting.

As data for the reaction rate, the hydrogen concentration and the temperature are known for any given point in time during the experimental trials, it is then possible to plot a point in 3-dimensional space for which the x, y, and z coordinates are the values for those three parameters at a specific time.

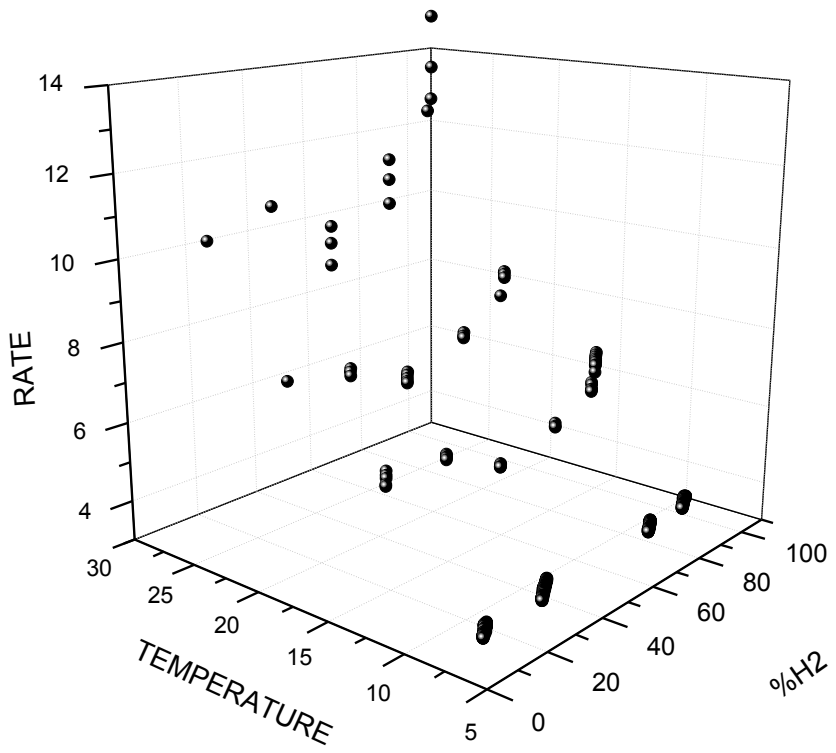

Figure 4-3 3-dimensional plot of flow rate, hydrogen concentration and temperature

This 3-dimensional plot is shown in Figure 4-3. The x and y axes respectively indicate the temperature and hydrogen concentration, and the z axis indicates the reaction rate. The surface created by the data points is a graphical indication of the relationship of R = f(T,C) as given in equation 2-2.

However, as a corresponding R value does not exist for every possible combination of T and C, it is necessary to calculate a fitting equation which represents the surface created by the data points with a reasonable degree of accuracy. Commercial data analysis software such as OriginPro or Excel offer various numerical approaches to accomplish this, such as plane, polynomial 2D, exponential 2D, Lorenz 2D and Gauss 2D fitting.

While different fitting equations might be suited for data obtained from other materials, for the TiCrV-Fe material used in this study we employ the polynomial 2D fitting function, which results in an equation with the formula

$$z = z0 + ax + by + cx2 + dy2 + fxy \qquad (4\text{-}1)$$

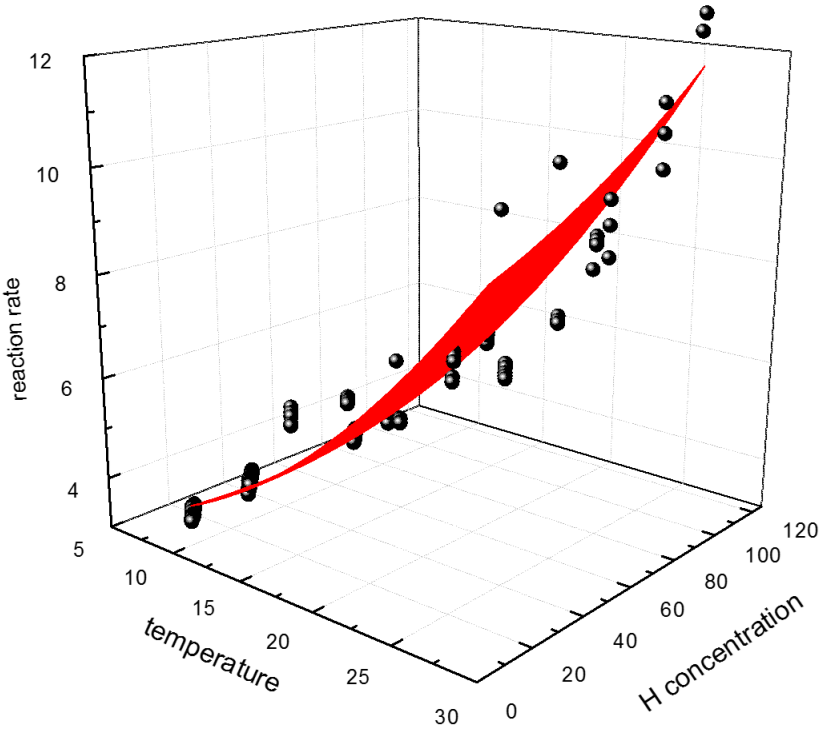

Figure 4-4 Fitting surface for 3-dimensional plot of flow rate, hydrogen concentration and temperature

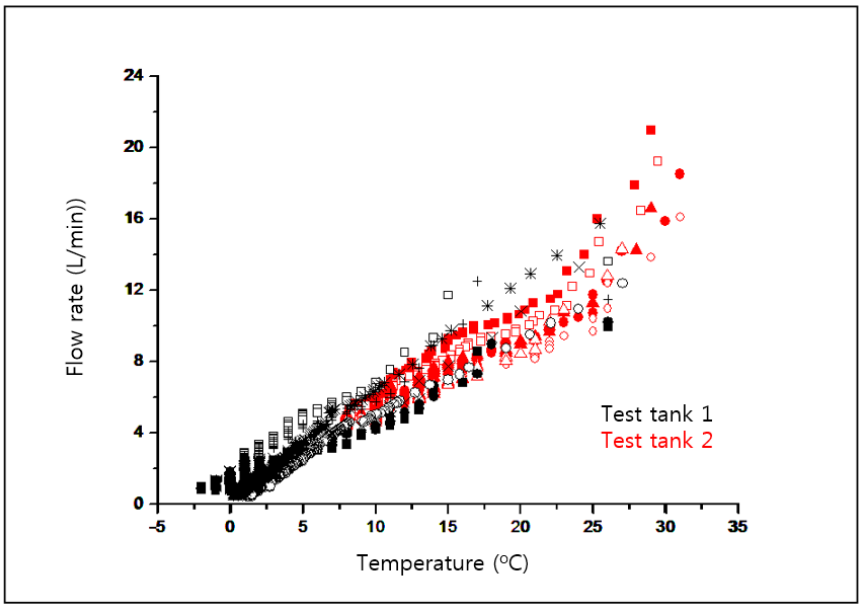

Figure 4-5 Dependence of flow rate on temperature

which results in a fitting surface as shown in Figure 4-4. This then becomes the basis for Equation 2-1 which is applied to the numerical model.

Simplified 2D fitting

It is worth noting that for some materials, including the TiCrV alloy used in the present study, the variable C is found to have only a negligible effect on the reaction rate. This can be seen in Figure 4-5, which is a plot of the measured flow rate versus the temperature, comprising data from both of the two different experimental tanks used in the study. Although the influence of the hydrogen concentration has been omitted, a clear trend is immediately evident, that the flow rate is strongly dependent on the temperature.

A closer observation of the data does reveal a significant variation of flow rates corresponding to a single given temperature. The data shows that the higher values for the flow rate at a given temperature correspond to higher hydrogen concentration. As the concentration decreases through multiple experimental trials, the flow rates also decrease slightly, as in Figure 4-6. An

explanation of this trend can be found by re-visiting the P-C isotherm.

A generalized representation of the P-C isotherm is shown in Figure 4-7. When the hydrogen concentration is high, the larger pressure differential between the equilibrium desorption pressure and the release pressure acts as a stronger driving force for the desorption reaction. However, as the hydrogen concentration, this pressure differential becomes smaller, so that the reaction occurs less readily.

For the TiCrV alloy used in the present study, the impact of the hydrogen concentration on the flow rate is relatively small. This is likely due to two factors. First, the system pressure is relatively low. Second, the desorption plateau is relatively flat, meaning that the equilibrium pressure during desorption is close to constant.

Hence, it is reasonable in some cases to omit C from the relationship in equation 2-1 and instead define the reaction rate in the form of equation 2-2, or R = f(T). In such a case, instead of the fitting surface equation in 3D data fitting, there would be a fitting line or curve for the 2D data, as in Figure 4-8.

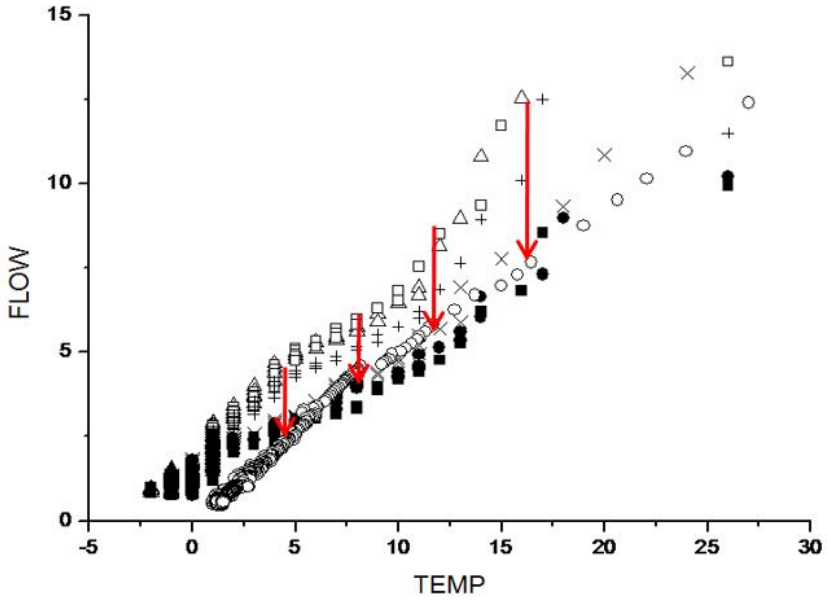

Figure 4-6 Decrease in flow rate at given temperature for lower hydrogen concentration

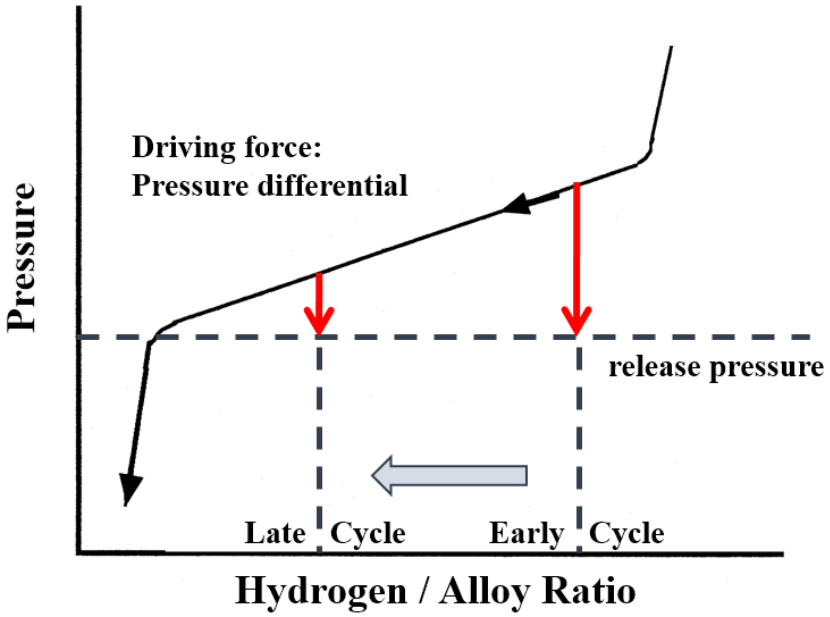

Figure 4-7 Schematic illustration of impact of hydrogen concentration on reaction rate

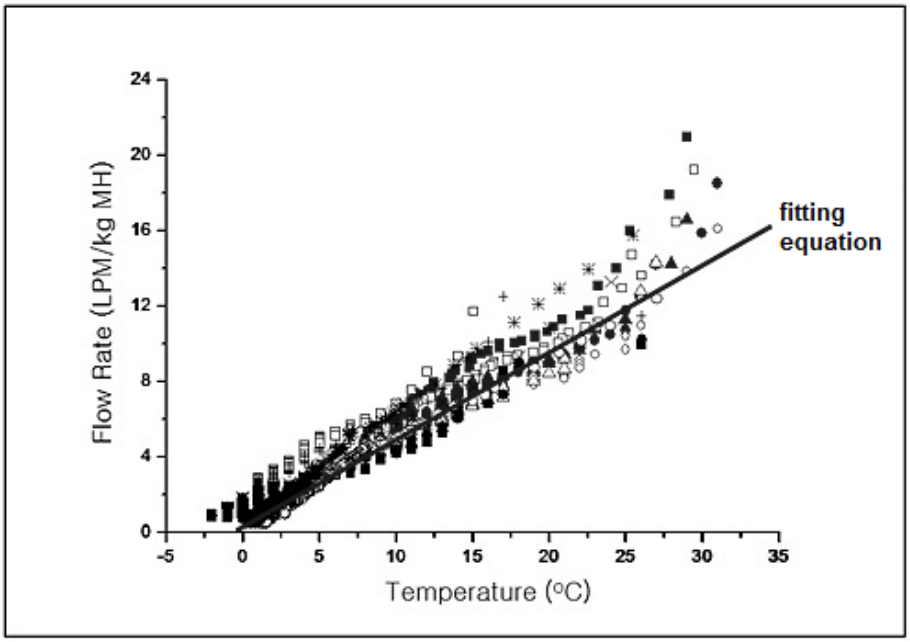

Figure 4-8 Fitting line/curve for 2-dimensional plot of flow rate and temperature

4.2 Experimental vs. calculated results

Despite the logic of the calculation algorithm, calculated results from the numerical model must be compared against measured results from a corresponding pilot system in order to verify the model's accuracy.

Figure 4-9 shows the measured vs. calculated reaction rate over time for two trials with flow limited to 5 slpm from each tank, for a total of 10 slpm. The temperature at the pilot tank's external wall was kept constant at 30 ^{o}C for one trial and 40 ^{o}C, for the other. This served a dual function. First, the heat from the wall, when transferred to the MH material, could sustain the desorption reaction for a longer period of time. Secondly, the constant wall temperature serves as a convenient boundary condition for the numerical model, making it easier to compared calculated and measured results.

In each case, the flow rate is initially maintained at the limited value. However, as the endothermic reaction gradually lowers the overall system temperature, eventually the system reaches a point at which the alloy temperature results in a lower reaction rate which can no longer support the designated flow rate, and

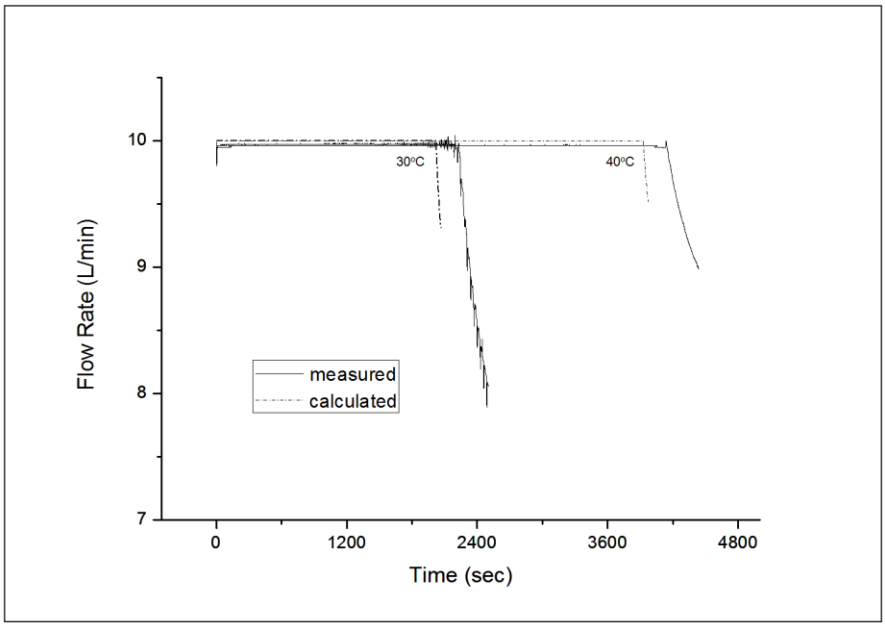

Figure 4-9 Measured and calculated flow rate over time for pilot tank system

the flow rate drops after that point. For both of the external heating conditions, this trend is expected, and shown to demonstrate good agreement between measured and calculated results.

However, for both cases it is clear that the measured results indicate a longer period during which the designated flow rate is maintained by the system, before the flow rate diminishes to below the designated value. In both cases, that difference in time during which the flow rate is maintained between measured and calculated results is found to be approximately 300 sec, or 5 minutes. That this time difference is nearly identical despite different experimental conditions indicates that the value arises from a factor which the two tanks share in common.

Given a porosity of approximately 0.49 for the MH alloy powder and the dimensions of the tank, roughly 1.4L in combined volume exists within the tanks which is not filled by the powder itself; in other words, that volume is filled by free gas which has not reacted with or from the powder. Given the initial hydrogen charging process, this results in approximately 50L of free gas

which is released from the tank prior to reaction and release from the MH alloy, which fits accurately with the 5 minutes of gas flow at 10LPM, the gap between the calculated and experimental results.

In short, the discrepancy in the calculated vs. experimental results was a result of a failure to take into account the free gas which is released from the tanks regardless of reaction from the MH alloy. The amount of this initial release of free gas prior to MH alloy reaction will depend on the dimensions of the tank, and the temperature and pressure conditions of the initial charge.

Taking into account this additional factor, we add the expected period of gas release at the designated flow rate to the initial point of the simulation, which gives us a much better agreement between calculated and measured results. Figure 4-10 shows results of measurement and calculation for gas release with the initial, non-reactive gas release from the early stages of the trials taken into account. In these results, we find that the calculated and measured values are indeed in excellent agreement.

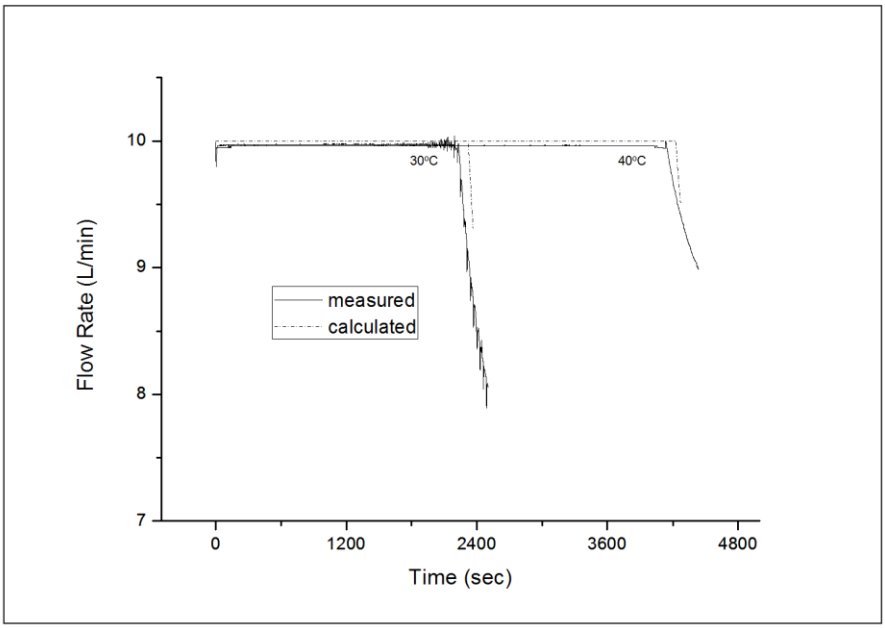

Figure 4-10 Measured and calculated flow rate over time for pilot tank system, taking into account unreacted free gas

This agreement between the measured and calculated results was repeatedly confirmed in multiple trials with different operating conditions. Figure 4-11 shows measured and calculated results for the length of time during which hydrogen is released from the pilot tank at the user-designated flow rate limit. The user-designated flow rate was set at 3.5 or 5.0 LPM. The external heating temperature was varied at 30, 40 and 50 ^{o}C. Again, the measured and calculated results are remarkably similar.

The closeness of the results calculated by the numerical model and measured from the pilot tank system demonstrates that the model is reliable and accurate. It may therefore be employed in a variety of applications, to be detailed in the subsequent chapter.

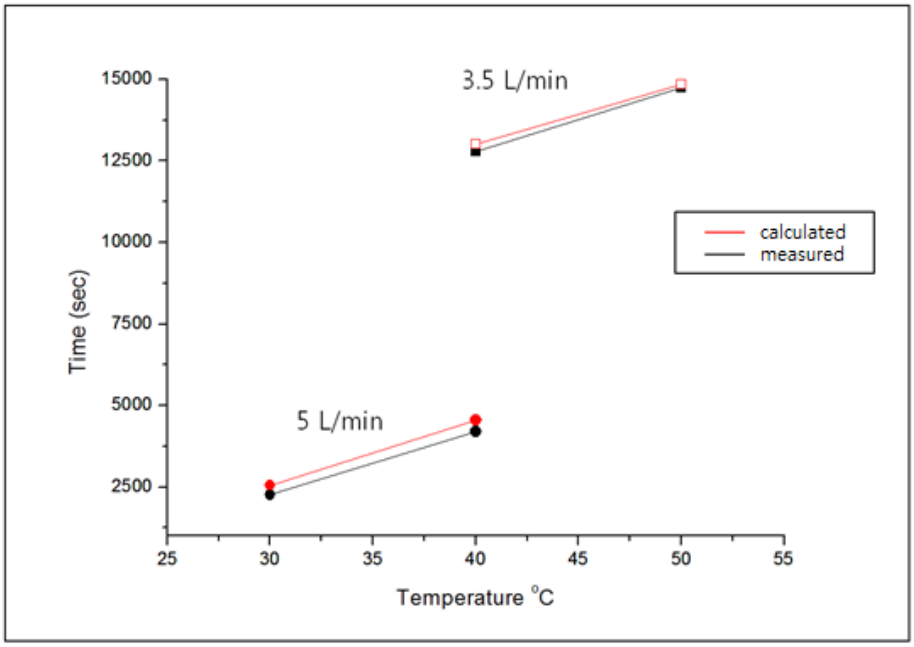

Figure 4-11 Measured and calculated time during which hydrogen is released at user-designated flow rate and various heating conditions.

Chapter 5. Model Applications

The numerical model, developed and verified through process described in previous chapters, can be employed to analyze and predict the desorption behavior in a variety of applications. Examples of such applications of the model are given in this chapter.

One application is the prediction of how a single fixed MH hydrogen storage vessel design will perform under various operating conditions. The operating conditions may include parameters such as the desired flow rate (ex. for use in fuel cell power generation). The effect of thermal control of a vessel on its performance through measures such as heaters or heat exchangers may also be useful in evaluating its suitability for use in a given system.

Another application of the model is to create a suitable design for an MH hydrogen storage vessel, given conditions for its use. Engineering concerns for a hydrogen tank include issues such as the capacity, weight, dimensions and expected flow rate. For any combination of such parameters, countless different structures or designs may be proposed. It would be very useful to be able to

predict the behavior of multiple candidate designs in order to determine the one most suitable for the application in question. The model developed in the present study provides a convenient way to do so.

5.1 Desorption behavior for a MH hydrogen storage vessel

5.1.1 Analysis of thermal behavior

In addition to the prediction of a vessel's ability to release hydrogen gas, as demonstrated in the process of verifying the model's accuracy in the previous chapter, the model can also be used to calculate temperature changes within a vessel during its operation. This can be especially useful when assessing a tank's design or considering ways to improve it, since an understanding of temperature changes which are difficult to measure directly can offer valuable clues regarding possible modifications.

The model in this study allows for calculation of the temperature variation in an MH hydrogen storage vessel during its operation both locally and as an overall average. While the average temperature value will determine the overall reaction and flow rates, it is also worth noting that there will be local variations of temperature depending on the location within the tank geometry. The present model allows for time-dependent calculation of these local temperature differences.

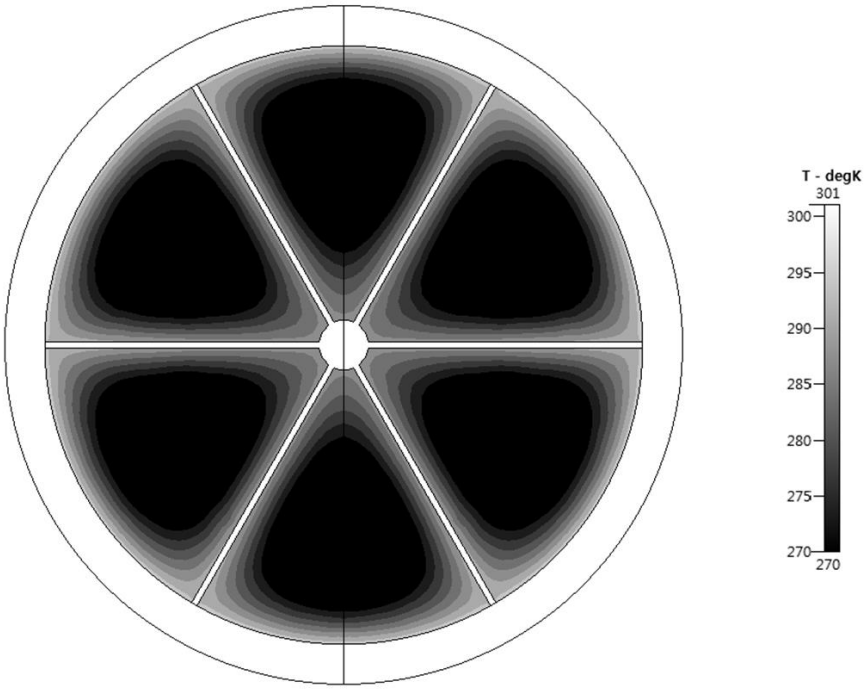

Figure 5-1 Cross section of pilot tank with temperature distribution in MH region

An example of this is given in Figure 5-1, which shows a cross section of the pilot tank with temperature given for the MH region at the point in time at which the temperature can no longer support the designated flow rate. It is worth noting that temperatures higher than the average can be found near the tank wall, and near the high-conductivity interior fins, as these areas allow heat to be transferred more readily from the surface heater to the MH region. In contrast, the regions of MH furthest from the tank wall and high-conductivity fins are seen to have relatively lower temperatures. From this observation, we can conclude that the overall variation of local temperature in an MH bed will depend on the tank geometry, and consequently the tank geometry plays a major role in the desorption behavior of an MH system.

5.1.2 Desorption behavior under multiple operating conditions

Given the reliability of the model as demonstrated through comparison with experimental results, the model can be used to predict desorption behavior for various operation conditions such as designated flow rate and heating

temperature.

Figure 5-2 is an expansion of the data used to verify the model's accuracy. It shows calculated values for the percentage of the total hydrogen capacity of the MH alloy in the pilot tank which is released at the designated flow rate, for additional combinations of external temperature and designated flow rate. This illustrates the model's ability to predict desorption behavior from a single tank under multiple operating conditions.

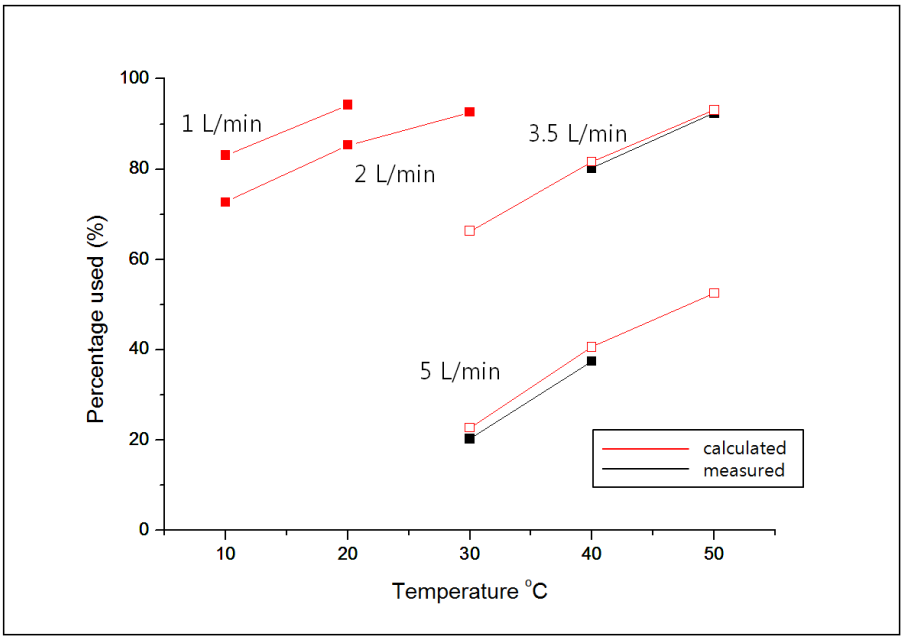

Figure 5-2 Calculated percentage of total hydrogen capacity of the pilot tank which is released at designated flow rate under various operating conditions

5.2 Analysis of multiple vessel designs for an engineering application

For many applications of hydrogen storage in MH materials, certain parameters for the vessel will be fixed. These factors may include the total capacity, weight, dimensions and expected flow rate. The model in the present study enables prediction of multiple vessel designs that fit the given criteria, so that the most suitable one may be selected.

Vessel designs

Figure 5-3 shows three different potential MH tank designs for automotive application, both schematically and as calculation grids. The major criteria for the tank, as outlined by a domestic carmaker, are given in Table 5-1 [80].

Figure 5-3 (a) is an illustration of Tank 1. It is a cylindrical tank with 160mm inner diameter and 186 mm inner length. The cylinder's exterior consists of a stainless steel liner which is 5mm thick, giving a total tank diameter of 170mm. Caps on either end of the cylinder result in a total tank

Category	Specification
Capacity	0.1 kg H_2
Alloy material	BCC (Ti-Cr-V)
Alloy mass	10 kg
Flow rate	20-25 LPM
Max. Pressure	5 MPa
Max. Temperature	70^{o}C
Cooling type	Tube (SUS) – Fin (Al)
Tank material	SUS
Tank type	Cylinder (+carbon fiber)

Table 5-1 Technical specifications for HMC automotive application tank designs

length of 206mm. In order to facilitate the transfer of heat between the inner MH region and the exterior of the tank, copper heat transfer plates measuring 1mm thick are added to the tank at 10mm intervals, result in 17 spaces between them which are filled with the MH alloy.

Figure 5-3 (b) is an illustration of Tank 2. Like Tank 1, it is cylindrical in shape but with different aspect ratios. Tank 2 has an inner diameter of 60mm and inner length of 1180mm. It also consists of a stainless steel exterior liner measuring 5mm thick. Tank 2 contains no inner heat transfer elements such as copper plates, as the thinner shape is expected to allow for easier transfer of heat between the tank's interior MH regions and the surface.

Figure 5-3 (c) is an illustration of Tank 3. Like Tanks 1 and 2, it is cylindrical in shape. It also has the same inner and outer radius as Tank 1, as well as approximately the same aspect ratio. However, in addition to the copper heat transfer plates, there are also tubes through which heated or cooled water or appropriate fluid may pass in order to facilitate heat transfer to or from the MH bed.

Tank 1	
MH alloy	10kg
Cooling method	int. plates and ext. convection
Total weight	15,386g
Weight % H_2	0.65% (1%alloy)

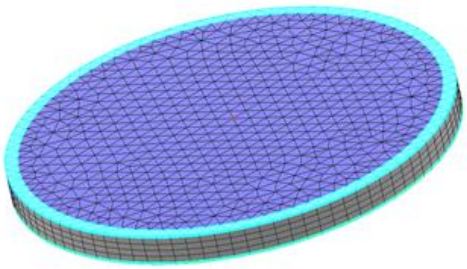

Figure 5-3(a) Potential MH tank designs for automotive application

Tank 2	
MH alloy	10 kg
Cooling method	ext. convection
Total weight	14,895 g
Weight % H_2	0.67% (1%alloy)

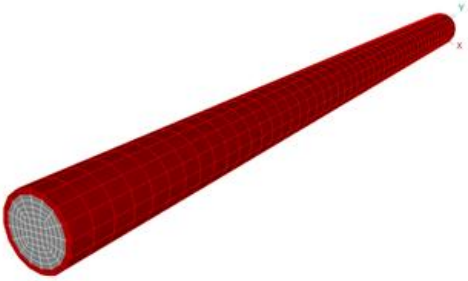

Figure 5-3(b) Potential MH tank designs for automotive application

Tank 3	
MH alloy	10 kg
Cooling method	ext. convection and fluid circuit
Total weight	15,607g
Weight % H_2	0.64% (1%alloy)

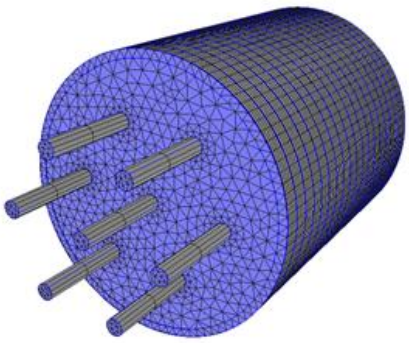

Figure 5-3(c) Potential MH tank designs for automotive application

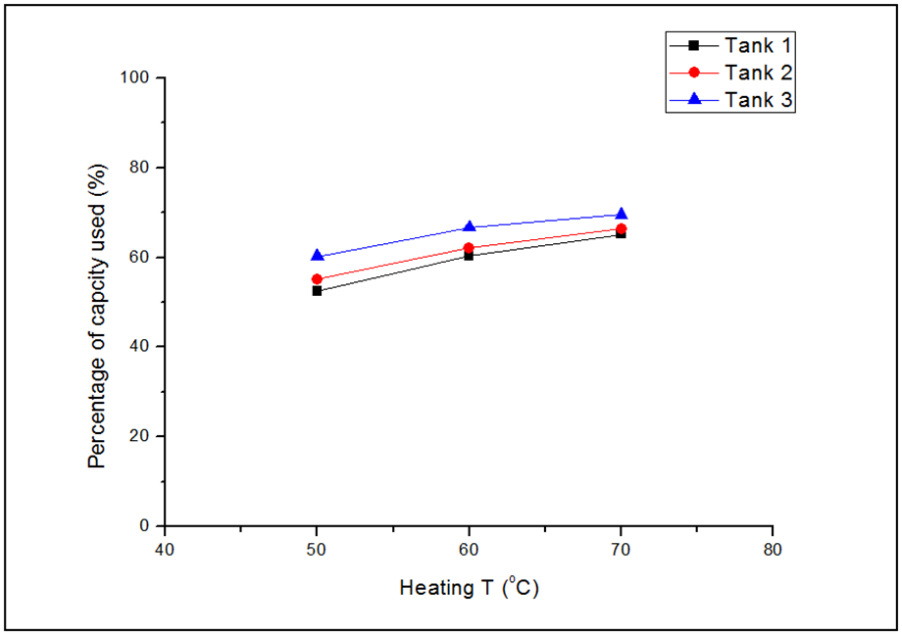

Figure 5-4 Projected temperature dependence of three tank designs

Calculated results

Figure 5-4 shows the projected temperature dependence of the three tank designs. The percentage of the total hydrogen capacity of each tank provided at the user designated flow rate of 10 LPM is plotted against the external heating temperature.

The results indicate that in general, a higher external temperature results in prolonged flow at the user designated rate, as the greater amount of heat provided allows the system to maintain that flow rate for a longer period of time. Naturally, this also allows systems at higher temperature to provide a greater percentage of the total stored hydrogen at the user-designated flow rate.

In terms of tank design, Tank 3 is predicted to be most effective in terms of hydrogen desorption at the user designated flow rate. This is to be expected given the tank's design, with its greater emphasis on heat transport in the tank's interior. Tanks 1 and 2 are shown to be relatively less efficient than Tank 3. While Tank 2 is predicted to be only marginally more effective than Tank 1, its relatively simpler structure may also be taken into account when

considering actual manufacturing and production.

The figure also indicates that the sensitivity of the tanks to the external temperature is greater at lower temperatures, regardless of design. This is demonstrated by the greater slope of the percentage of hydrogen used versus external heating temperature at lower temperatures. However, at higher temperatures, the impact of the heating temperature on the percentage of the hydrogen released at the user designated flow-rate diminishes. This can be attributed to the inherent inability of the tank geometry and particularly of the properties of the MH material to transport heat from the tank surface to the interior.

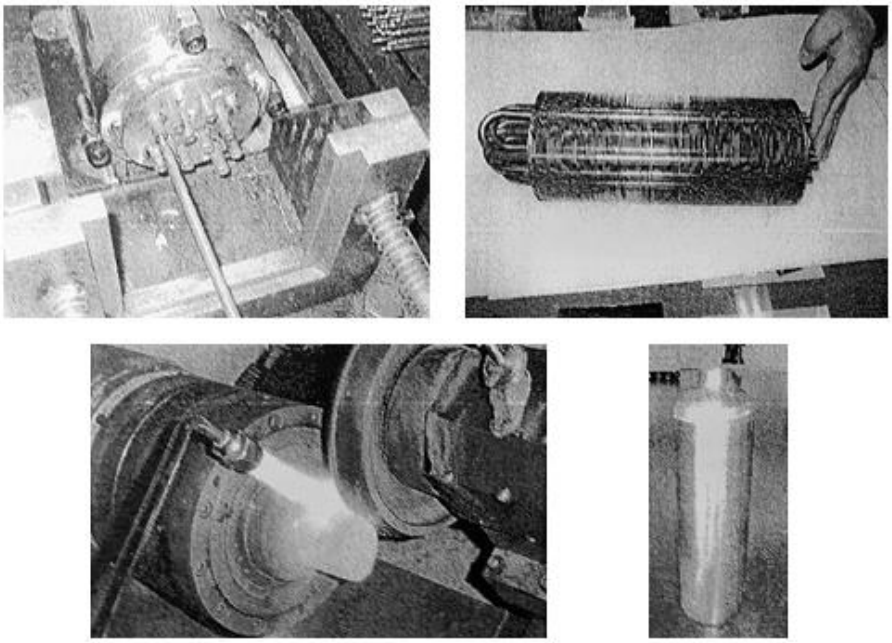

Figure 5-5 Manufacturing process of MH hydrogen storage vessel

Comparison with direct experimentation

The domestic carmaker which designated the tank criteria used in this section built an actual vessel based on those criteria and performed direct measurements of its desorption behavior. The process of building the vessel, shown in Figure 5-5, illustrates the relative convenience and need for an accurate numerical model.

Figure 5-6 shows the results of direct experimentation on the tank for a trial in which the external temperature is 60 ^{o}C and the user-designated flow rate is 10 LPM. Figure 5-7 shows the flow rate over time for the three tanks described above, under identical operating conditions. The measured data indicate that the designated flow rate is maintained for approximately 83 minutes. This is remarkably close in value to the roughly 78 minutes calculated for tank 3, which is nearly identical in design to the experimental tank.

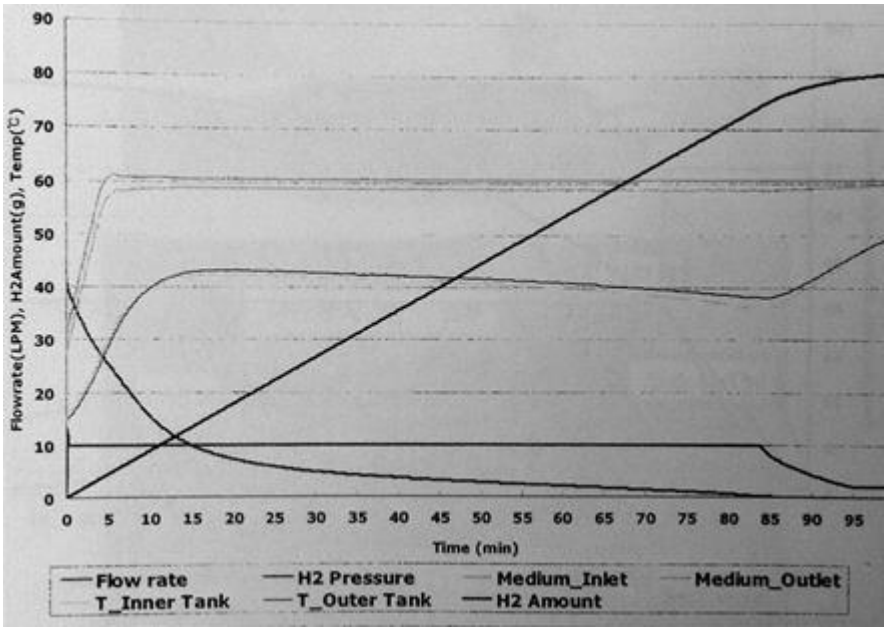

Figure 5-6 Experimental results for manufactured MH hydrogen storage vessel

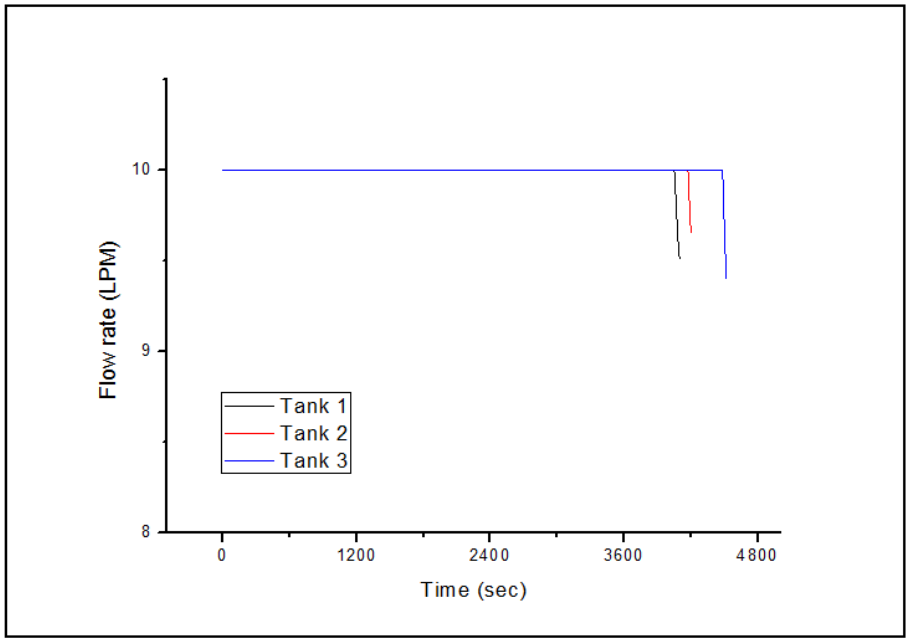

Figure 5-7 Calculated flow rate over time for three tanks

Temperature results and qualitative design evaluation

Figure 5-8 shows the calculated 3D temperature distribution within tanks 1 (a), 2 (b) and 3 (c), for the point at which the flow rate drops below the user-designated value. The high porosity of the bed and diffusivity of hydrogen results in a relatively uniform reaction rate throughout the bed, and consequently a relatively uniform temperature distribution.

The main source of heat for the endothermic desorption reaction is the external heater which is wrapped around the device surface for all three cases. For tank 3, additional heat is transported to the device interior through the heat exchange fluid circuits.

Qualitatively, it can be seen that the temperature is mostly uniform and low throughout the hydride bed, and high only at the regions of the bed located closest to the sources of heat. This is due to the low effective thermal conductivity of the bed, arising from its high porosity. This 3D heat distribution can offer valuable clues regarding how the design can be improved to facilitate heat transfer.

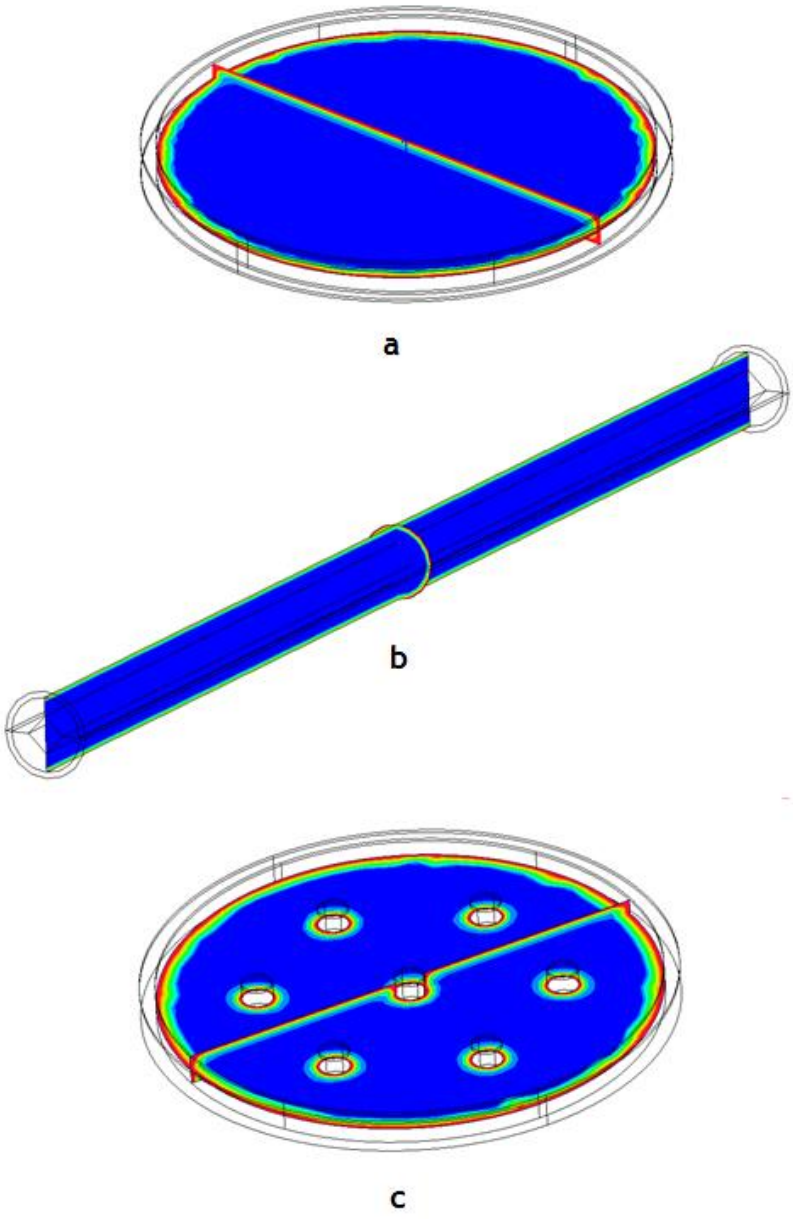

Figure 5-8 Calculated 3D temperature distribution in three tank designs for qualitative design evaluation

Chapter 6. Conclusions

A numerical model was developed in the present study to analyze desorption behavior in metal hydride hydrogen storage systems. The model presents a novel approach to characterizing the desorption behavior of a hydrogen storage alloy through experimentation.

The hydrogen flow rate from a material and its temperature during desorption is measured through experimentation. This also yields the change in hydrogen concentration over the same period of time. Rearranging these data results in a 3-dimensional set of points whose coordinates are the three measured parameters. It is possible through data fitting to create a surface which approximates this set of points. The equation which defines the surface characterizes the relationship between the three parameters to give the reaction rate as a function of hydrogen concentration and temperature, or $R = f(T,C)$.

By applying this relationship to the numerical model, it is possible to calculate the change in reaction rate, temperature and hydrogen concentration over time, both locally and for the system as a whole. The implementation of

an additional variable, dubbed the rate factor ‘k’ and defined as the ratio between the potential and real rates of reaction, makes it possible to calculate desorption behavior for the likely presence of a user-designated flow rate limit.

Experimentation on a pilot scale tank of TiCrV-Fe alloy and numerical analysis of the tank using the algorithm above yields results which are in very good agreement. This verifies the accuracy of the model.

As the model is demonstrated to be accurate, it can be used in a variety of applications. The model may be used to predict the desorption behavior of a given MH tank under various operating conditions. It can also be used to evaluate the performance of multiple tank designs which fit specific engineering criteria, so that the most appropriate one may be identified.

Taken together, the accuracy of the model and the versatility of its application makes it a promising and useful tool for the analysis, evaluation and design of metal hydride hydrogen storage systems.

References

[1] M. Ball and M. Wietschel, “The Hydrogen Economy: Opportunities and Challenges”, Cambridge University Press, 1st ed. (2009).

[2] E. Tzimas, C. Filiou, S.D. Peteves and J.-B. Veyret, “Hydrogen Storage: State-of-the-art and Future Perspective”, Mission of the Institute for Energy, European Commission, Directorate General Joint Research Centre, The Netherlands (2003).

[3] IEA, “Hydrogen Production and Storage: R&D Priorities and Gaps”, IEA Publications (2006)

[4] S. A. Sherif, F. Barbir, and T.N. Veziroglu, “Principles of hydrogen energy production, storage and utilization”, J. of Scientific & Industrial Research, 62, 46-63, (2003).

[5] A. Zuttel, “Materials for hydrogen storage”, Materials Today, 6, 24-33 (2003).

[6] A. Niedzwiecki, Storage, Presentation at DoE Hydrogen Vision Meeting, Washington, D.C., November 15-16, (2001).

[7] R.S. Irani, “Hydrogen storage: high-pressure gas containment”, MRS Bulletin, 27, 680-682 (2002).

[8] ”GM 700 bar hydrogen storage breakthrough extends FCV range”, Fuel Cells Bulletin, 2003, 9, (2003).

[9] J. Wolf, “Liquid-hydrogen technology for vehicles”, MRS Bulletin, 27, 684-

687 (2002).

[10] L. Schlapbach, A. Zuttel, “Hydrogen storage materials-mobile applications”, Nature, 414, 353-358 (2001).

[11] G. Sandrock, “Hydrogen Metal Systems and Applications of Hydrides”, in Hydrogen Energy Systems, Production and Utilization of Hydrogen and Future Aspects”, Y. Yurum, ed. Kluwer Publishing, (2005).-

[12] G. Sandrock, “A panoramic overview of hydrogen storage alloys from a gas reaction point of view”, J. Alloys and Compounds, 293-295, 877-888 (1999).

[13] J. C. Moreno-Pirajan, “Thermodynamics - Interaction Studies - Solids, Liquids and Gases”, Intech, 1st ed. (2011)

[14] L. Klebanoff and J. Keller, “5 years of hydrogen storage research in the US DOE metal hydride center of excellence (MHCoE)”, Int. J. Hydrogen Energy, 38, 4533–4576 (2013).

[15] L. Klebanoff and J. Keller, “Final Report for the DOE Metal Hydride Center of Excellence”, Sandia National Laboratories (2012).

[16] T. Sakai, I. Uehara, H. Ishikawa, “R&D on metal hydride materials and Ni–MH batteries in Japan”, J. of Alloys and Compounds, 293–295, 762-769 (1999).

[17] P.D. Goodell, “Stability of rechargeable hydriding alloys during extended cycling”, J. of the Less Common Metals, 99, 1-14 (1984).

[18] R.L. Cohen, K.W. West and K.H.J. Buschow, “Degradation of hydrogen-

absorbing rare earth intermetallics by cycling", Solid State Communications, 25, 293-295 (1978).

[19] R.L. Cohen and K.W. West, "Intrinsic cycling degradation in LaNi5 and annealing procedures for re-forming the material", J. of the Less Common Metals, 95, 17–23 (1983).

[20] G. Sandrock and G. Thomas, IEA/DOE/SNL Hydride Databases, Internet URL http://hydpark.ca.sandia.gov

[21] I. Jacob, J.M. Bloch, D. Shaltiel and D. Davidov, "On the occupation of interstitial sites by hydrogen atoms in intermetallic hydrides: A quantitative model", Solid State Communications, 35, 155-158 (1980)

[22] D. Shaltiel, "Hydride properties of AB_2 laves-phase compounds", J. of the Less Common Metals, 73, 329-338 (1980).

[23] T. Gamo, Y. Moriwaki, N. Yanagihara, T. Yamashita and T. Iwaki, "Formation and properties of titanium-manganese alloy hydrides", Int. J. of Hydrogen Energy, 10, 39-47 (1985).

[24] T. Gamo, Y. Moriwaki, N. Yanagihara and T. Iwaki, "Life properties of Ti Mn alloy hydrides and their hydrogen purification effect", J. of the Less Common Metals, 89, 495-504 (1983).

[25] A.R. Miedema, K.H.J. Buschow and H.H. Van Mal, "Which intermetallic compounds of transition metals form stable hydrides?, J. of the Less Common Metals, 49, 463-472 (1976).

[26] H. A. Kierstead, P.J. Viccaro, G.K. Shenoy and B.D. Dunlap, "Pressure-

composition phase diagram for hydrides of rare earth-Fe2 laves compounds", J of the Less Common Metals, 66, 219-222 (1979).

[27] H. A. Kierstead, "The hydrides of YFe2 and GdFe2", J of the Less Common Metals, 86, L1-L4 (1982).

[28] O. Bernauer, "Metal hydride technology", Int. J. of Hydrogen Energy, 13, 181-190 (1988).

[29] O. Bernauer and C. Halene, "Properties of metal hydrides for use in industrial applications", J. of the Less Common Metals, 131, 213-224 (1987).

[30] D. Ivey and D. Northwood, "Hydrogen site occupancy in AB2 Laves phases", J. of the Less Common Metals, 115, 23-33 (1986).

[31] K.C. Hoffman, J.J. Reilly, F.J. Salzano, C.H. Waide, R.H. Wiswall and W.E. Winsche, "Metal hydride storage for mobile and stationary applications", Int. J. of Hydrogen Energy, 1, 133-151 (1976).

[32] B. Abrashev, T. Spassov, S. Bliznakov and A. Popov, "Microstructure and electrochemical hydriding/dehydriding properties of ball-milled TiFe-based alloys", Int. J. of Hydrogen Energy, 35, 6332-6337 (2010).

[33] B.-H. Liu, "Hydrogen–Metal Systems: Hydride Forming Alloys (Properties and Characteristics, Database Information), Encyclopedia of Materials: Science and Technology, 2nd ed. (2001).

[34] A. J. Maeland, "Investigation of some new hydride systems", J. of the Less Common Metals, 89, 173-182 (1983).

[35] G. Sandrock, “State-of-the-Art Review of Hydrogen storage in Reversible Metal Hydrides for Military Fuel Cell Applications”, Final Report for ONR Contract N00014-97-M-0001, NTIS Order No. AD-A328 073/2INZ

[36] H. Iba and E. Akiba, “Hydrogen absorption and modulated structure in Ti–V–Mn alloys”, J. of Alloys and Compounds, 253–254, 21–24 (1997).

[37] S.W. Cho, C.S. Han, C.N. Park and E. Akiba, “The hydrogen storage characteristics of Ti–Cr–V alloys”, J. of Alloys and Compounds, 288, 294–298 (1999)

[38] A. Kamegawa, T. Tamura, H. Takamura and M. Okada, “Protium absorption–desorption properties of Ti–Cr–Mo bcc solid solution alloys”, J. of Alloys and Compounds, 356–357, 447–451 (2003).

[39] K. Kubo, H. Itoh, T. Takahashi, T. Ebisawa, T. Kabutomori, Y. Nakamura and E. Akiba, “Hydrogen absorbing properties and structures of Ti–Cr–Mo alloys”, J. of Alloys and Compounds, 356–357, 452–455 (2003).

[40] S.W. Cho, C.S. Han, C.N. Park, and E. Akiba, “Hydrogen storage characteristics of Ti–Zr–Cr–V alloys”, J. of Alloys and Compounds, 289, 244–250 (1999).

[41] Y. Tominaga, S. Nishimura, T. Amemiya, T. Fuda, T. Tamura, T. Kuriiwa, A. Kamegawa and M. Okada, “Protium Absorption-Desorption Properties of Ti–V–Cr Alloys with a BCC Structure”, Materials Transactions, JIM, 40, 871-874 (1999).

[42] S.W. Cho, H. Enoki and E. Akiba, “Effect of Fe addition on hydrogen

storage characteristics of Ti0.16Zr0.05Cr0.22V0.57 alloy", J. of Alloys and Compounds, 307, 304–310 (2000).

[43] Y. Tominaga, K. Matsumoto, T. Fuda, T. Tamura, T. Kuriiwa, A. Kamegawa, H. Takamura and M. Okada, "Protium Absorption-Desorption Properties of Ti–V–Cr–(Mn, Ni) Alloys", Materials Transactions, JIM, 41, 617-620 (2000).

[44] X.B. Yu, , Z. Wu, B.J. Xia and N.X. Xu, "Enhancement of hydrogen storage capacity of Ti–V–Cr–Mn BCC phase alloys", J. of Alloys and Compounds, 372, 272–277 (2004).

[45] X.B. Yu, Z. Wu and N.X. Xu, "Effects of melt-quenching rates on the hydrogen storage properties of Ti-based BCC phase alloy", Physica B: Condensed Matter, 344, 456–461 (2004).

[46] S.W. Cho, H. Enoki, T. Kabutomori, C.N. Park and E. Akiba, "Isotope effect on structural transitions of Ti1.0Mn0.9V1.1HX(DX) and Ti1.0Cr1.5V1.7HX(DX) with hydrogenation", J. of Alloys and Compounds, 319, 196–203 (2001).

[47] S.W. Cho, C.N. Park, J.H. Yoo, J. Choi, J.S. Park, C.Y. Suh and G. Shim, "Hydrogen absorption–desorption characteristics of Ti(0.22 + X)Cr(0.28 + 1.5X)V(0.5 − 2.5X) ($0 \leq X \leq 0.12$) alloys", J. of Alloys and Compounds, 403, 262–266 (2005)

[48] P. Muthukumar, M. P. Maiya and S. S. Murthy, "Experiments on a metal hydride-based hydrogen storage device", Int. J. of Hydrogen Energy, 30,

1569-1581 (2005).

[49] M. Gambini, M. Manno and M. Vellini, “Numerical analysis and performance assessment of metal hydride-based hydrogen storage systems”, Int. J. of Hydrogen Energy, 33, 6178-6187 (2008).

[50] B. D. MacDonald and A. M. Rowe, “Impacts of external heat transfer enhancements on metal hydride storage tanks”, Int. J. of Hydrogen Energy, 31, 1721-1731 (2006).

[51] B. D. MacDonald and A. M. Rowe, “A thermally coupled metal hydride hydrogen storage and fuel cell system”, J. of Power Sources, 161, 346-355 (2006).

[52] T. Oi, K. Maki and Y. Sakaki, “Heat transfer characteristics of the metal hydride vessel based on the plate-fin type heat exchanger”, J. of Power Sources, 125, 52-61 (2004)

[53] S.S. Bedbak and M. Ram Gopal, “Performance analysis of a compressor driven metal hydride cooling system”, Int. J. of Hydrogen Energy, 30, 1127 – 1137 (2005).

[54] M. Nagel, Y. Komazaki, and S. Suda, “Effective thermal conductivity of a metal hydride bed augmented with a copper wire matrix”, J. of Less-Common Metals, 120, 35-43 (1986).

[55] H.-P. Klein and M. Groll, “Heat transfer characteristics of expanded graphite matrices in metal hydride beds”, Int. J. of Hydrogen Energy, 29, 1503-1511 (2004).

[56] R. W. Rice, “Evaluation and extension of physical property-porosity models based on minimum solid area”, J. of Materials Science, 31, 102-118 (1996).

[57] S. Tarafdar, A. Franz, C. Schulzky, and K. H. Hoffmann, “Modelling porous structures by repeated Sierpinski carpets”, Physica A, 292, 1–8 (2001).

[58] K. Kaviany, “Principles of Heat Transfer in Porous Media”, Springer 1995).

[59] J. Zhang, T. S. Fisher, P. V. Ramachandran, J. P. Gore and I. Mudawar, “A review of heat transfer issues in hydrogen storage technologies,” J. of Heat Transfer, 127, 1391-1399 (2005).

[60] A. Sarkar, and R. Banerjee, “Net Energy Analysis of Hydrogen Storage Options”, Int. J. of Hydrogen Energy, 30, 867–877 (2005).

[61] D. L. Anton, D. A. Mosher and S. M. Opalka, “High Density Hydrogen Storage System Demonstration Using NaAlH4 Complex Compound Hydrides”, Proceedings of the 2004 Annual U.S. DOE Hydrogen Program Review (2004).

[62] A. Rodriguez Sanchez, H.-P. Klein and M. Groll, “Expanded Graphite as Heat Transfer Matrix in Metal Hydride Beds”, Int. J. of Hydrogen Energy, 28, 515–527 (2003).

[63] K. J. Kim, B. Montoya, A. Razani and K.-H. Lee, “Metal Hydride Compacts of Improved Thermal Conductivity”, Int. J. of Hydrogen Energy, 26, 609–613 (2001).

[64] S. A. Gadre, A. D. Ebner, S. A. Al-Muhtaseb and J. A. Ritter, “Practical Modeling of Metal Hydride Hydrogen Storage Systems”, Industrial & Engineering Chemistry Research, 42, 1713–1722 (2003).

[65] Y. Asakum, S. Miyauchi, T. Yamamoto, H. Aoki and T. Miura, “Homogenization Method for Effective Thermal Conductivity of Metal Hydride Bed”, Int. J. of Hydrogen Energy, 29, 209–216 (2004).

[66] J. Wang, “Hydride Development for Hydrogen Storage”, Proceedings of the 2004 Annual U.S. DOE Hydrogen Program Review (2004).

[67] Y. A. Buyevich, “On the thermal conductivity of granular materials”, Chemical Engineering Science, 29, 37-48 (1974).

[68] A. D. Brailsford and K. G. Major, “The thermal conductivity of aggregates of several phases, including porous materials”, Brit. J. of Applied Physics, 15, 313-319 (1964).

[69] W. Schotte, “Thermal Conductivity of Packed Beds”, AIChE Journal, 6, 63-67 (1960).

[70] A. Kurt and H. Ates, “Effect of porosty on thermal conductivity of powder metal materials”, Materials and Design, 28, 230-233 (2007).

[71] X. Huai, W. Wang and Z. Li, “Analysis of the effective thermal conductivity of fractal porous media”, App. Thermal Engineering, 27, 2815-2821 (2007).

[72] Y. Asakum, S. Miyauchi, T. Yamamoto, H. Aoki and T. Miura, “Numerical Analysis of Absorbing and Desorbing Mechanism for the Metal Hydride

by Homogenization Method", Int. J. of Hydrogen Energy, 28, 529–536 (2003).

[73. T. Nakagawa, A. Inomata, H. Aoki and T. Miura, "Numerical Analysis of Heat and Mass Transfer Characteristics in the Metal Hydride Bed", Int. J. of Hydrogen Energy, 25, 339–350 (2000).

[74] F. Askri, A. Jemni and S.B. Nasrallah "Prediction of Transient Heat and Mass Transfer in a Closed Metal-Hydrogen Reactor", Int. J. of Hydrogen Energy, 29, 195–208 (2004).

[75] Z. Guo and H. J. Sung, "Technical Note Conjugate Heat and Mass Transfer in Metal Hydride Beds in the Hydriding Process", Int. J. of Heat Mass Transfer, 42, 379–382 (1999)

[76] CFD-ACE+ v.2014.0 Modules Manual

[77] CFD-ACE+ v.2014.0 User Manual

[78] S.-W. Cho, G. Shim, G.-S. Choi, C.-N. Park, J.-H. Yoo and J. Choi, "Hydrogen absorption–desorption properties of Ti0.32Cr0.43V0.25 alloy", J. of Alloys and Compounds, 430, 136-141 (2007).

[79] J.-H. Yoo, G. Shim, S.-W. Cho and C.-N. Park, "Effects of desorption temperature and substitution of Fe for Cr on the hydrogen storage properties of Ti0.32Cr0.43V0.25 alloy", Int. J. of Hydrogen Energy, 32, 2977 – 2981 (2007).

[80] Hyundai Motor Company, "Development of metal hydride hydrogen storage materials and small scale storage systems for a fuel cell vehicle",

report for Ministry of Educational Science and Technology, Republic of Korea (2009).

초록

금속 수소화물 (MH) 합금은 저압에서의 사용과 높은 저장용량이 가능한 수소저장 재료이다. 그러나 합금의 수소저장 특성을 개선하기 위한 연구는 활발하게 진행되고 있는 반면, 이러한 합금을 사용한 대용량 수소저장 용기에 대한 연구는 상대적으로 미비한 실정이다. 특히 수소와 금속 재료간의 반응에서 발생하는 반응열에 의한 온도 변화는 저장 특성에 크게 영향을 미치기 때문에 고용량 저장 용기는 이를 반영할 필요가 있다.

본 연구에서는 금속 수소화물을 사용한 수소저장 시스템의 설계 및 평가를 위한 수치모델을 제시한다. 합금의 수소 방출 거동을 시간에 따른 온도, 반응 속도, 그리고 수소 농도의 변화를 기준으로 측정한다. 측정된 데이터를 분석하여 이들 변수간의 관계를 도출하고, 그 관계를 바탕으로 합금 시스템의 복합 전산모사 모델을 구축한다. 본 연구에서는 실측 데이터를 얻기 위해 TiCrV-Fe 합금을 사용하지만, 실험 방법은 해석하고자 하는 대부분의 금속 수소화물에 동일하게 적용이 가능하다.

모델을 통해 계산된 결과는 실제 측정 결과와 정확하게 일치하는 것으로 확인되었다. 이 같은 모델의 정확성은 다양한 환경과 작동 조건에서 특정 시스템의 수소 방출 거동 예측을 가능하게 한다. 또한 주어진 작동 조건을 충족시키는 다양한 시스템의 비교 분석 및 평가도 가능하다.

본 연구에서 구축한 전산모델은 정확도와 활용도가 높아 다양한 구조, 규모 및 사용 재료에 따른 수소저장 시스템의 분석에 사용이 가능할 것으로 보인다.

주요 단어 : 수소 저장, 금속 수소화물, 수치 해석,
수치 모델링, 전산 모사

학 번 : 2006-20859